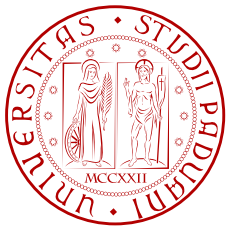


UNIVERSITY OF PADOVA

DEPARTMENT OF INFORMATION ENGINEERING


Ph.D. Course in Information Engineering

*Curriculum:* Bioengineering

*Series:* XXIX

# Quantitative analysis of hypoglycemia-induced EEG alterations in type 1 diabetes


*Course director:*
Prof. Matteo BERTOCCO

*Coordinator:*
Prof. Giovanni SPARACINO

*Ph.D. candidate:*
Maria RUBEGA

*Advisor:*
Prof. Giovanni SPARACINO


A thesis submitted in fulfillment of the requirements
for the degree of Philosophiae Doctor

January 31, 2017

*"Nanos gigantum humeris insidentes."*

Bernardus Carnotensis

*"If I have seen further, it is by standing on the shoulders of giants."*

Isaac Newton

# *Abstract*

The main risk for patients affected by type 1 diabetes (T1D) is to fall in hypoglycemia, an event which leads to both short and long-terms automatic failure and can be life-threatening especially when occurs at night without subject awareness. Moreover, T1D patients can develop asymptomatic hypoglycemia, reducing the prompt response of the counterregulatory system triggered by the fall in blood glucose. Avoiding hypoglycemia is important in children and adolescents because hypoglycemia episodes may have clinically relevant effects on cognition. Also in adults, cognitive tests assessed that hypoglycemia results in altered cerebral activity, most likely due to the complete dependence of the brain for glucose supply.

The first organ influenced by this fall of glucose in the blood is the brain. Indeed, a lot of studies proved the mirroring of cognitive dysfunction due to hypoglycemia in the spectral power of the electroencephalogram (EEG) signal. In particular, the increase of the power in low frequency EEG bands is a well-known effect during hypoglycemia that seems more pronounced in the EEG recording in the posterior areas of the brain. Pilot studies about the real-time processing of the EEG signal to detect hypoglycemia have indicated that it might be possible to alert the patients by means of EEG analysis. The main advantages in exploiting EEG analysis is that the blood glucose threshold to enter in hypoglycemia has large inter-subjects variations, on the contrary the EEG onset in general occurs before the state of hypoglycemia is critical, i.e., the brain starts to experience neuroglycopoenia and its functions completely fail.

The main aim of this work is to broaden out the quantitative analysis on the altered EEG activity due to hypoglycemia in T1D patients to identify potential margins of improvement in EEG processing and further features sensitive to hypoglycemia. In particular, the analyses are extended to different domains, i.e., time and frequency domains, to deepen the knowledge on the effects of hypoglycemia in the brain. So far, studies in the literature have mainly evaluated these changes only on a single EEG channel level on the frequency domain, but limited information is available on the hypoglycemia influence on brain network dynamics and on connection between different brain areas. To do so, this dissertation is structured in 7 chapters, briefly presented below.

Chapter 1 will start with a brief overview about the impact of T1D and its main effects on daily life. Moreover, the main consequences of hypoglycemia in human brain will be described by reporting the main findings in the literature.

Chapter 2 will present the database where EEG data and blood glucose samples were collected in parallel for about 8 h in 31 T1D hospitalized patients during an hyperinsulinemic – hypoglycemic clamp experiment.

Chapter 3 will address on the main effects of hypoglycemia in the frequency domain. After testing the well-known changes in the spectral power of the EEG signal during hypoglycemia, a multivariate analysis based on the concept of Information Partial Directed Coherence will be presented. In particular, we will confirm the general slowing in the frequency domain and we will show how hypoglycemia affects the EEG functional connectivity.

Chapter 4 will consider the effects of hypoglycemia on EEG complexity. Fractal dimension features, describing both amplitude and frequency properties, will be computed and compared

with the results based on Sample Entropy. We will reveal a decrease of EEG signal complexity in the hypoglycemic condition.

Chapter 5 will focus on the consequences of hypoglycemia in the so-called microstates or "athoms of thought". We will hypothesize that the changes in the frequency domain and the decrease of the EEG signal complexity in hypoglycemia have in common the same resting EEG electric potential amplitude map.

Chapter 6 will describe how hypoglycemia influences the results of cognitive tests, and the relationship between the drop in the tests performance and the EEG quantitative measures presented in the previous chapters. We will find a direct correlation among the changes in the power spectra, the cognitive tests performance and the changes of one resting EEG electric potential amplitude map.

Eventually, Chapter 7 will close the dissertation by interpreting the ensemble of the results from both the medical and engineering point of view, and presenting the possible future developments of this work.

# *Sommario*

Il principale rischio per i pazienti colpiti dal diabete di tipo 1 (T1D) è cadere in ipoglicemia, un evento che provoca una nutrita serie di sintomi ed effetti a breve e lungo termine e può essere particolarmente pericoloso quando si verifica durante la notte senza averne coscienza. Inoltre, questi pazienti rischiano di sviluppare una forma di ipoglicemia senza sintomi, riducendo la risposta ormonale controregolatoria innescata dalla diminuzione della concentrazione di glucosio nel sangue. Evitare questo stato patologico, è particolarmente importante sia nei bambini e adolescenti per evitare possibili distorsioni cognitive, sia negli adulti dove test cognitivi hanno dimostrato un'alterata condizione cerebrale durante l'ipoglicemia. Infatti l'ipoglicemia provoca una diminuzione delle funzioni cerebrali e l'organo maggiormente affetto da questo stato patologico è il cervello.

Si trovano vari studi in letteratura che provano come la riduzione delle funzioni cognitive si rifletta in cambiamenti della potenza spettrale del segnale elettroencefalografico (EEG). In particolare, la crescita della potenza delle basse frequenza nel segnale EEG è un effetto ben noto in letteratura. Studi pilota hanno dimostrato che potrebbe essere possibile utilizzare il segnale EEG per segnalare l'entrata in ipoglicemia. Il maggiore vantaggio è che se la soglia di concentrazione di glucosio nel sangue è variabile da soggetto a soggetto, l'onset dei cambiamenti del segnale EEG avviene solitamente prima che lo stato di ipoglicemia sia così grave da causare una marcata neuroglicopenia con conseguente disfunzione cerebrale.

Il principale scopo di questa tesi è approfondire l'analisi delle alterazioni del segnale EEG nel T1D causate dall'ipoglicemia per identificare potenziali margini di miglioramento nell'analisi del segnale EEG e ulteriori caratteristiche sensibili all'ipoglicemia. In particolare, le analisi sono estese a diversi domini, il dominio del tempo e il dominio della frequenza, per approfondire la conoscenza sugli effetti dell'ipoglicemia sul cervello. Fino ad ora, gli studi in letteratura hanno principalmente valutato questi cambiamenti a livello di singolo canale EEG e nel dominio della frequenza, ma una limitata informazione è disponibile sull'influenza dell'ipoglicemia sulla dinamica della rete cerebrale e sulla connessione tra le diverse aree cerebrali. Per affrontare questi temi, la tesi è strutturata in 7 capitoli, brevemente descritti di seguito.

Il Capitolo 1 presenta una panoramica sulle conseguenze e sull'impatto nella vita di tutti i giorni del T1D. Inoltre, si descrivono brevemente i risultati sugli effetti dell'ipoglicemia sull'attività cerebrale riportati in letteratura.

Il Capitolo 2 riporta il database su cui sono basate tutte le analisi presentate in questa tesi. Il segnale EEG e la concentrazione di glucosio nel sangue sono state raccolte in parallelo per circa 8 ore in 31 pazienti ospedalizzati affetti da T1D indotti in ipoglicemia attraverso un clamp ipoglicemico iperinsulinemico.

Il Capitolo 3 tratta degli effetti dell'ipoglicemia sull'EEG nel dominio della frequenza. Dopo aver confermato la presenza di cambiamenti nel valore della potenza del segnale EEG durante l'ipoglicemia, si riporta un'analisi multivariata basata sulla stima della connettività funzionale del segnale EEG durante questo stato patologico. In particolare, confermeremo il rallentamento del segnale EEG nel dominio della frequenza e dimostreremo come lo stato ipoglicemico influenza la connettività funzionale del segnale EEG.

Il Capitolo 4 si concentra sugli effetti dell'ipoglicemia sulla

complessità del segnale EEG. In particolare, le analisi sono basate su indicatori frattali e sul confronto dei loro valori con i risultati di indicatori basati sulla definizione di entropia. Riveleremo una decrescita della complessità del segnale EEG durante lo stato di ipoglicemia.

Il Capitolo 5 tratta le conseguenze dello stato ipoglicemico sui microstati, definiti anche "atomi del pensiero". Ipotizzeremo che i cambiamenti nel dominio della frequenza e la decrescita della complessità del segnale EEG possano essere originati da una stessa mappa delle ampiezze del potenziale elettrico del segnale EEG.

Il Capitolo 6 si focalizza sull'influenza dell'ipoglicemia sui risultati di test cognitivi come lo Stroop test. Inoltre, tratta la relazione tra il calo nella performance in questi test e le misure quantitative del segnale EEG presentate nei capitoli precedenti. Troveremo una correlazione diretta tra i cambiamenti della potenza spettrale, dei test cognitivi e di una mappa EEG.

Infine, il Capitolo 7 conclude la tesi cercando di interpretare tutti i risultati nel dominio del tempo e della frequenza sia da un punto di vista clinico sia da un punto di vista ingegneristico e presenta i possibili sviluppi futuri.

# *Acknowledgements*

First of all, I would thank my advisor, Prof. Giovanni Sparacino, because my Phd "journey" was possible thanks to him and his support in the last three years. This Phd pursuing involves scientific curiosity, initiative and self-motivation, but also interpersonal and communication skills. All these important features for a "budding researcher" also improved thanks to my visiting experience in the cross-functional team of Prof. Christoph Michel. In particular, I would deeply thank my advisor in Geneva, Dr. Markus Gschwind, for his precious help and support during my stay. I learned a lot from him. But my Phd experience was amazing and unforgettable also thanks to all the new colleagues and friends I met in these three years: my colleagues in Padova, but also my temporary, but not least special, colleagues in Geneva. Thanks to all of you, you enriched me as a person and as a never-ending student!

Last but not least, I would like to thank my family for their unconditional support. In particular, my parents, key figures both in my education and in my life skills.

# Contents

# List of Figures

# List of Tables

# List of Abbreviations

| | |
|---|---|
| **AIC** | **A**kaike **I**nformation **C**riterion |
| **AUC** | **A**rea **U**nder the **C**urve |
| **BBB** | **B**lood-**B**rain **B**arrier |
| **BG** | **B**lood **G**lucose |
| **C** | **C**entral lobe |
| **CF** | **C**entroid **F**requency |
| **CGM** | **C**ontinuous **G**lucose **M**onitoring |
| **EEG** | **E**lectro**E**ncephalo**G**ram |
| **EU** | **EU**glycemia |
| **F** | **F**rontal lobe |
| **FC** | **F**unctional **C**onnectivity |
| **fMRI** | **f**unctional **M**agnetic **R**esonance **I**maging |
| **GEV** | **G**lobal **E**xplained **V**ariance |
| **GFP** | **G**lobal **F**ield **P**otential |
| **GMD** | **G**lobal **M**ap **D**issimilarity |
| **HAAF** | **H**ypoglycemia-**A**ssociated **A**utomatic **F**ailure |
| **HYPO** | **HYPO**glycemia |
| **ID** | **ID**entifier |
| **iPDC** | **I**nformation **P**artial **D**irected **C**oherence |
| **Lac** | **Lac**tate |
| **MANOVA** | **M**ultivariate **An**alysis **O**f **V**ariance |
| **MAR** | **M**ultivariate **A**uto**R**egressive |
| **MSE** | **M**ulti **S**cale **En**tropy |
| **NC** | **N**aming **C**olors |
| **NCWd** | **N**aming the **C**olors of the print of **W**ord**s** |
| **O** | **O**ccipital lobe |
| **P** | **P**arietal lobe |
| **p** | **p**-value |
| **PSD** | **P**ower **S**pectral **D**ensity |
| **RMS** | **R**oot **M**ean **S**quare |
| **ROC** | **R**eceiver **O**perating **C**haracteristic |
| **SampEn** | **Samp**le **En**tropy |
| **T** | **T**emporal lobe |

| | |
|---|---|
| **T1D** | **T**ype **1** **D**iabetes |
| **TMT** | **T**rail **M**aking **T**est |
| **TTC** | **T**otal **T**ime **C**overage |
| **YSI** | **Y**ellow **S**pring **I**nc |

*To my family*

# Chapter 1

# Hypoglycemia and EEG in type 1 diabetes

## 1.1 Type 1 diabetes and Hypoglycemia

### 1.1.1 The pathology of type 1 diabetes

The 5-10% of people suffering from diabetes are affected by type 1 diabetes (T1D) [1], also called juvenile diabetes because it is usually diagnosed in children or young adults. Nowadays the majority of individuals affected by T1D are adults, because of the rising number of new-onset cases of T1D in adults and the increased life expectancy for individuals with childhood-onset diabetes [2]. Type 1 diabetes is most common in Scandinavian populations and in Sardinia and Kuwait, and much less common in Asia and Latin America (data are generally lacking for sub-Saharan Africa and large parts of Latin America) [3]. In the past few decades, the annual incidence appears to be rising steadily by about 3% in high income countries [4] [5].

In this kind of disease, the autoimmune destruction of the $\beta$-cells of the pancreas results in the consequent insulin deficiency, leading to the subsequent increased glucose in blood and urine.

Insulin is the most potent anabolic hormone known, and promotes the synthesis and storage of carbohydrates, lipids and proteins, while inhibiting their degradation and release into the circulation. Insulin stimulates the uptake of glucose, i.e., the most important fuel for human metabolism, but also amino acids and fatty acids into cells, and increases the expression or activity of enzymes that catalyze glycogen, lipid and protein synthesis, while inhibiting the activity or expression of those that catalyze degradation [6]. To compensate the lack of insulin secretion, T1D patients are lifelong dependent on exogenous insulin. For a correct insulin administration, they need to self-monitor their blood glucose, diet, physiological insulin replacement, medication, and lifestyle in order to maintain good glycemic control, avoiding hypoglycemia, considered one of the most dangerous complications of diabetes treatment. Although current methods of blood glucose detection and insulin replacement have improved in the last years, e.g., by continuous glucose monitoring (CGM) devises and smart pumps [7], they are still imperfect and the hypoglycemia risk is high in T1D patients.

The internationally approved definition of symptomatic hypoglycemia is an event during typical neurogenic symptoms, such as shakiness, anxiety, nervousness, palpitations, sweating, dry mouth, pallor, and pupil dilation, are accompanied by a measure plasma glucose concentration lower than $70\ \mathrm{mg/dl}$ ($3.9\ \mathrm{mmol\,l^{-1}}$). The huge range of physiological, hormonal, symptomatic and cognitive responses triggered by the fall in blood glucose are visible in Fig. 1.1 [8]. All the neurogenic signs are caused by elevated levels of epinephrine, i.e., the primary fast-acting hormone in the defense against acute hypoglycemia, besides glucagon. However, epinephrine responses to hypoglycemia can become impaired in T1D [9], leading to hypoglycemia unawareness. Thus, T1D patients can develop a high risk to fall in asymptomatic

hypoglycemia, reducing further the efficacy of the counterregulatory responses to future hypoglycemia: a vicious cycle, Fig. 1.2. Nevertheless, hypoglycemia awareness can be reversed by avoiding new hypoglycemia episodes, thanks to a strict glycemic control.

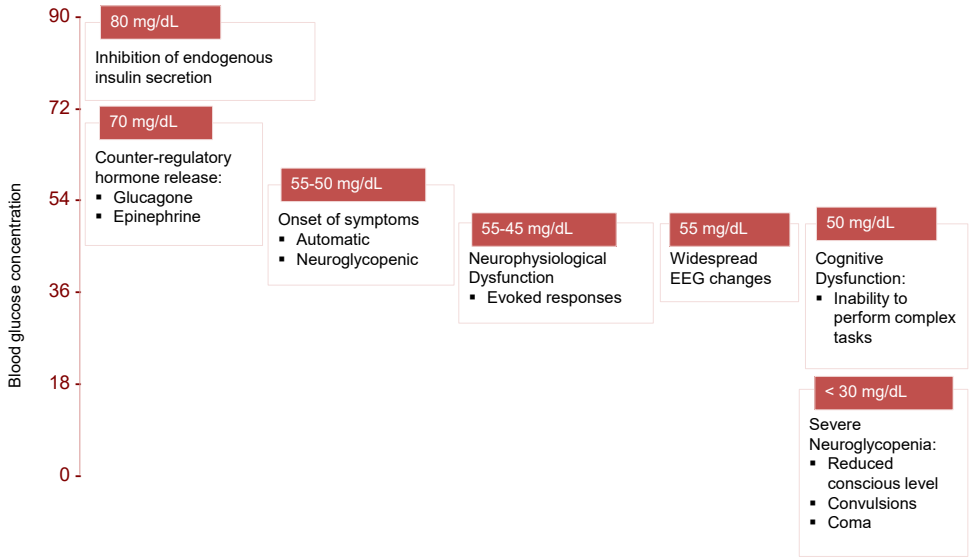


FIGURE 1.1: Glycemic thresholds for secretion of counter-regulatory hormones and onset of physiological, symptomatic, and cognitive changes in response to hypoglycemia in non-diabetic humans. Reproduced from [10].

### 1.1.2 Morbidity and mortality of hypoglycemia

Iatrogenic hypoglycemia causes recurrent physical and psychological morbidity and some mortality, impairs defenses against subsequent hypoglycemia, and precludes maintenance of euglycemia, i.e., blood glucose concentration in the range $[70 - 180]$

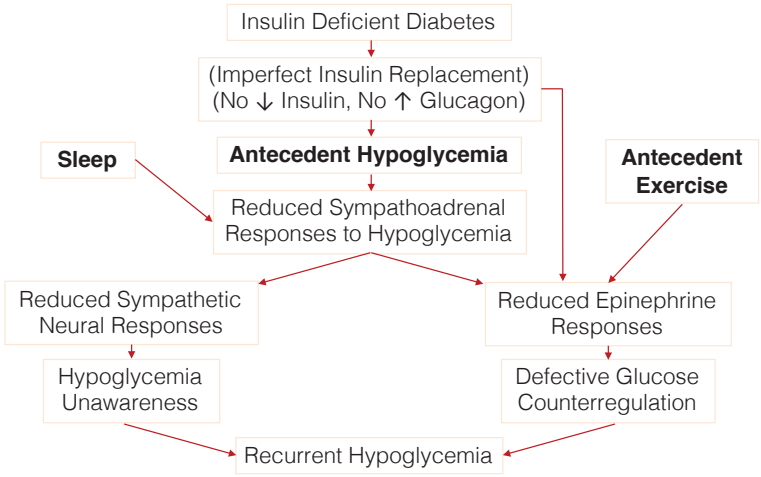


FIGURE 1.2: Schematic diagram of hypoglycemia-associated automatic failure (HAAF) in diabetes. Reproduced from [11].

$\mathrm{mg/dl}$ ($[3.9 - 10]$ $\mathrm{mmol\,l^{-1}}$), over a lifetime of diabetes [12]. In particular, hypoglycemia can have both short-term dangerous effects, such as cognitive dysfunction, behavioral abnormalities, confusional state, coma, seizures, transient ischaemic attack and transient hemiplegia, and long-term effects, such as cerebrovascular events, hemiparesis, focal neurological deficits, ataxia, choreoathetosis, cognitive impairment with behavioral and psychosocial problems and rarely, epilepsy and vegetative state [13]. To avoid diabetes complications and to guarantee a high quality of life, in a good diabetes self-management, special attention should be paid to diabetes-related distress, fear of hypoglycemia, eating disorders, insulin omission, subclinical depression, and clinical depression [2]. Moreover, physical activity and exercise may be very challenging for T1D patients because of the increasing risk of hypoglycemia during immediately, following and, about 7–11 h post-exercise, caused by muscles replenishing glycogen stores

post-exercise [2]. Last, but not least, sleep is a risk factor for nocturnal hypoglycemia that is very common, often asymptomatic and undetected [14]. During night, usual hypoglycemia warning symptoms and the sympatho-adrenal response are blunted [15], moreover the intensity of symptoms is diminished when lying flat [16].

As previously discussed, hypoglycemia has a wide-ranging clinical effects, but also social and economical in both industrialized and developing nations. Indeed, hospitalization of diabetic people after a hypoglycemic episode leads to a significant increase of treatment costs due to an increased length of hospital stay and a higher risk of all-cause mortality [17]. In conclusion, avoiding hypoglycemia in T1D is both medically and economically important.

## 1.2 Hypoglycemia and the brain

### 1.2.1 The role of glucose in brain function

Glucose is the main source of energy for human brain and its regulation is critical for brain physiology [18]. Despite the brain accounts for 2% of body weight, it is the principal consumer of glucose, i.e., 20% of glucose-derived energy [19]. In Fig. 1.3, the role of the glucose in human brain is summarized. In particular, specialized centers in the brain, including neurons in the hypothalamus, sense central and peripheral glucose levels and regulate glucose metabolism (panel A in Fig. 1.3). Glucose supply to the brain is regulated by neurovascular coupling and may be modulated by metabolism-dependent and -independent mechanisms (panel B in Fig. 1.3). Glucose enters the brain from the blood by crossing the blood-brain barrier (BBB) through glucose transporter 1, and glucose and other metabolites (e.g. lactate, Lac) are

rapidly distributed through a highly coupled metabolic network of brain cells (panel C in Fig. 1.3). Glucose provides the energy for neurotransmission (panel D in Fig. 1.3), and several glucose-metabolizing enzymes control cellular survival (panel E in Fig. 1.3) [18]. Indeed, glucose is required for both neurotransmitters synthesis and several glucose-metabolizing enzymes control cellular survival, but the largest amount of glucose is consumed for neural computation and signal processing, furthermore the brain increases its glucose consumption upon activation [20]. In particular, in adult brain, neurons have the highest energy demand and the BBB that separates the circulating blood from the brain extracellular fluid is highly selective and permeable for glucose. Thus, glucose is an energy source that is not replaceable for the brain.

### 1.2.2 Cognition dysfunction during hypoglycemia

The human brain depends on the continuous supply of glucose and it is vulnerable for any glucose deprivation. For this reason, the lack of glucose can lead to both-short term and long-term cognitive dysfunction. For instance, in a 16-year follow-up study [21], authors proved that T1D subjects early exposure to severe hypoglycemia episodes may have lasting and clinically relevant effects on cognition. Indeed, subjects with early severe hypoglycemia already had reduced cognitive function in childhood. Moreover, they also tended to have a less favorable development in cognitive function during follow-up compared with control subjects, in particular in memory (assessed by Rey Auditory Verbal Learning Test), problem solving and verbal function (assessed by Wechsler Adult Intelligence Scale III), and psychomotor efficiency (assessed by finger tapping). In [22], where cognitive tests, i.e., the California Computerized Assessment Package, the Stroop test and the Trail Making Test B (TMT B), were

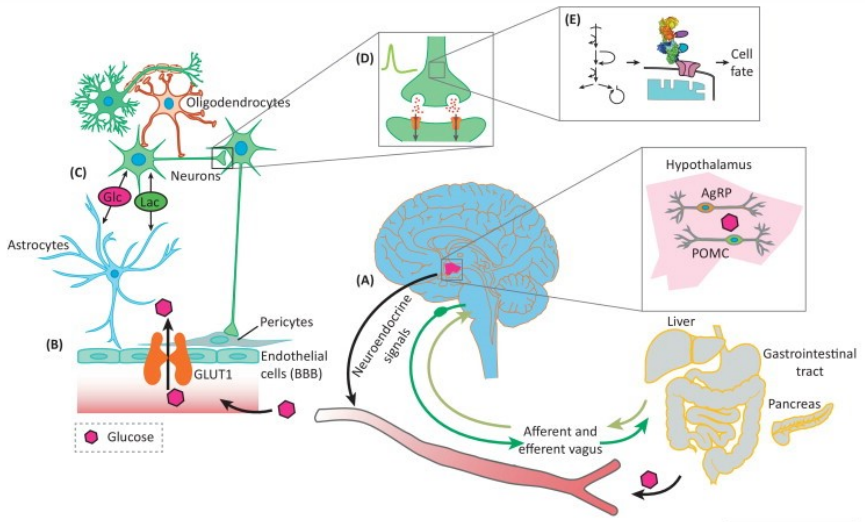


FIGURE 1.3: (A) Specialized centers in the brain sense central and peripheral glucose levels and regulate glucose metabolism. (B) Glucose supply to the brain is regulated by neurovascular coupling. (C) Glucose and other metabolites are rapidly distributed through a highly coupled metabolic network of brain cells. (D) Glucose provides the energy for neurotransmission, and (E) several glucose-metabolizing enzymes control cellular survival. Reproduced from [18]

performed to assess selective attention, visual attention, cognitive alterations, the reaction time and speed of information processing in T1D adults during hypoglycemia compared to euglycemia, cognitive function deteriorated as expected during hypoglycemia. In the above studies, cognitive tests assessed that hypoglycemia results in an altered cerebral activity, likely due to the entirely dependence of the brain for glucose supply. Therefore, the brain is the first organ to be affected by hypoglycemia and the decrease of cerebral functioning consequent to this condition may be investigated through suitable analysis of the electroencephalogram (EEG) signal.

### 1.2.3 Hypoglycemia-related EEG changes

The EEG signal is the recording from multiple electrodes of the brain electrical activity made along the scalp in standard locations according, for example, with the 10/20 International System, where each site has a letter to identify the lobe and a number to identify the hemisphere, i.e., letters F, T, C, P and O stand for frontal (yellow area in Fig. 1.4), temporal (blue area), "central", parietal (green area), and occipital lobes (orange area), respectively and even numbers refer to electrode positions on the right hemisphere, while odd numbers refer to those on the left hemisphere. In Fig. 1.5, a representative example of a sweep of a single EEG channel recording (P3-A1A2) in the time domain is depicted: the amplitude is about tens of $\mu$V, the signal is not periodic, but has some dominant rhythms. Indeed, in the frequency domain, the EEG signal can be seen as the sum of simpler parts characterized by different frequency components as described in panel (a) in Fig. 1.6: delta waves, from 1 to 4 Hz, characterized by high amplitude waves; theta waves, from 4 to 8 Hz, that appear during meditative and relaxed state in adults; alpha waves, from 8 to 13 Hz, that appear with closing eyes and decrease during mental efforts and opening eyes; and beta waves, from 13 to 30 Hz, that represent thinking, active concentration and movements. We can evaluate how the energy of the EEG signal is distributed with frequency observing its power spectrum, panel (b) in Fig. 1.6.

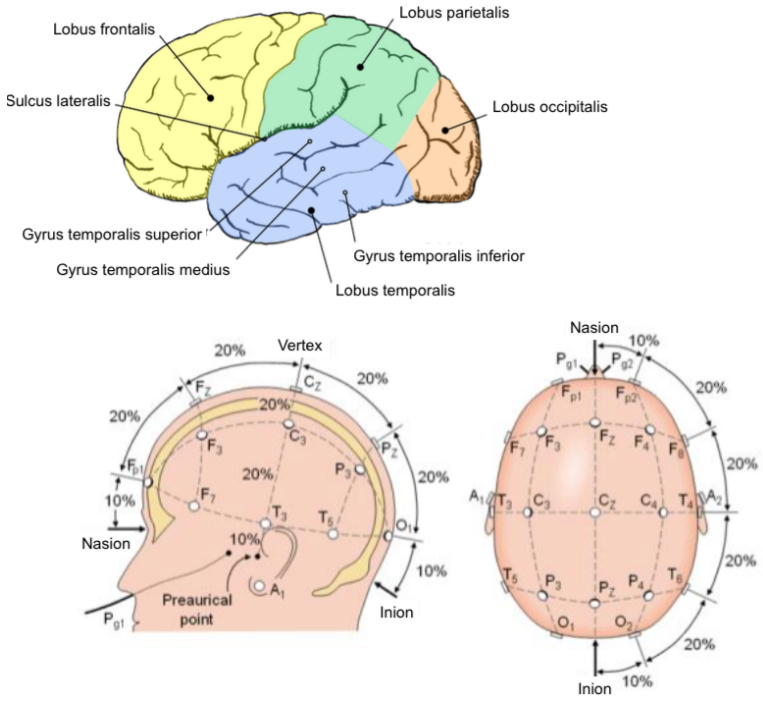


FIGURE 1.4: Brain lobes (upper panel) and standardize nomenclature and location of electrodes in the 10/20 International System (lower panel).

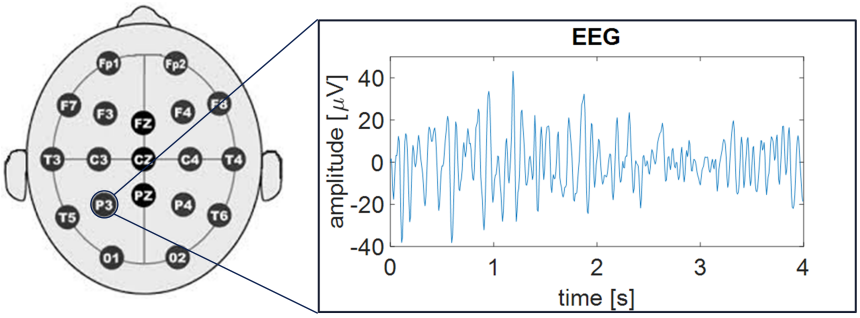


FIGURE 1.5: Representative example of a 4-s EEG sweep from P3-A1A2 derivation in the time domain.

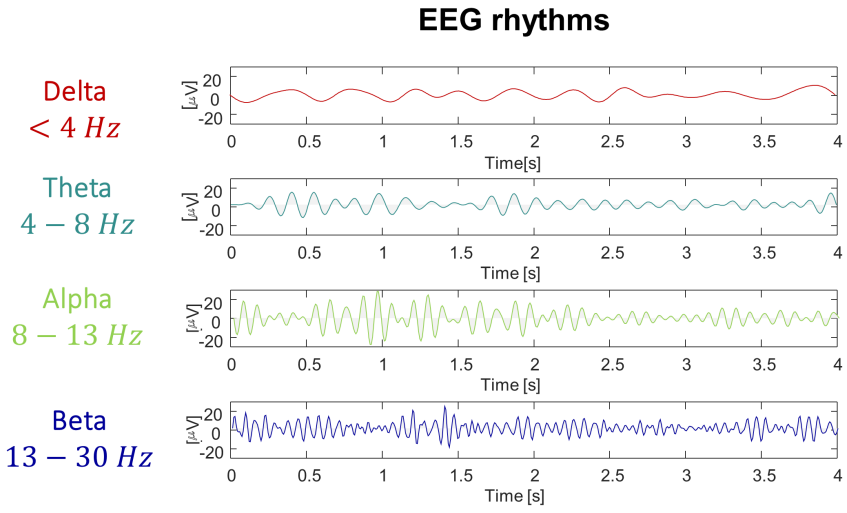


(a)

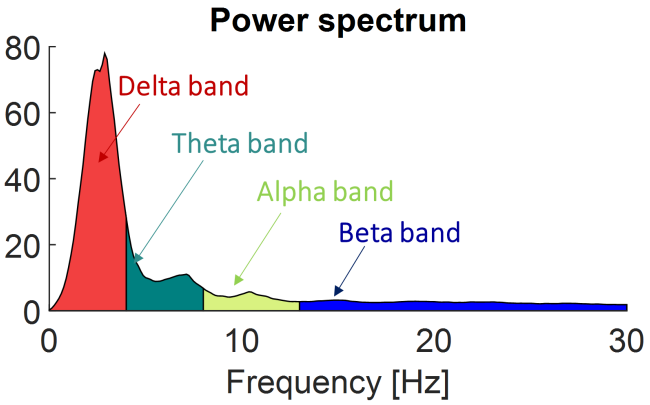


(b)

FIGURE 1.6: (a) Main frequency components of the EEG signal represented in Fig. 1.5; (b) power spectrum of the same signal.

Hypoglycemia causes an extensive range of clinical effects and highly affects the brain functions. Indeed, hypoglycemic events in patients with T1D are associated with measurable EEG changes. The first studies aiming to see if cognitive dysfunction was mirrored by altered EEG activity during hypoglycemia date back to 40's: in [23], authors observed abnormal EEG activity defined as slow potentials, high amplitudes fast potentials and irregular or disorganized patterns, during hypoglycemia. Then, also in [24], authors emphasized the importance of blood sugar concentration on cerebral function, observing EEG dysrhythmia, i.e., distorted EEG waves with higher amplitude, during hypoglycemia, as visible in Fig. 1.7. But hypoglycemia-effect on EEG was also quantified by the increase of low-frequency slow-wave activity [25]. For instance, in [26], the hypoglycemic condition was correlated with an increase in the theta activity in diabetic children and in [27], pathological activity in both delta and theta bands was observed in T1D adolescents. This increase in the power of low frequency bands during hypoglycemia in T1D patients is a well-established effect in the literature. Indeed, in [28], authors observed an increase in theta activity set in abruptly at a mean blood glucose concentration close to $2\ \mathrm{mmol\,l^{-1}}$. These changes were symmetrically and diffusely spread over the cortex though slightly more pronounced in the recordings from the temporal and parieto-occipital areas. In [29], induced hypoglycemia in eight T1D patients resulted in a significant increase in low frequency electroencephalographic activity, most pronounced over anterior regions of the brain. After the hypoglycemic period, EEG activity was normalized immediately. Also in [30], an increase in delta, and especially in theta activity was found by showing a topographic maximum in lateral frontal regions during light hypoglycemia ($[50-60]\ \mathrm{mg/dl}$), while during deep hypoglycemia

(40 mg/dl) there was a topographic maximum of slow frequencies in posterior parts of the brain (centro-temporal to parieto-occipital regions). In [31], similar results were found in adolescents with T1D, where a history of severe hypoglycemia correlated with a global increase in theta activity, whereas poor metabolic control correlated with elevated delta activity. Moreover, a decrease in fast activity was most pronounced bilaterally in the posterior temporal regions.

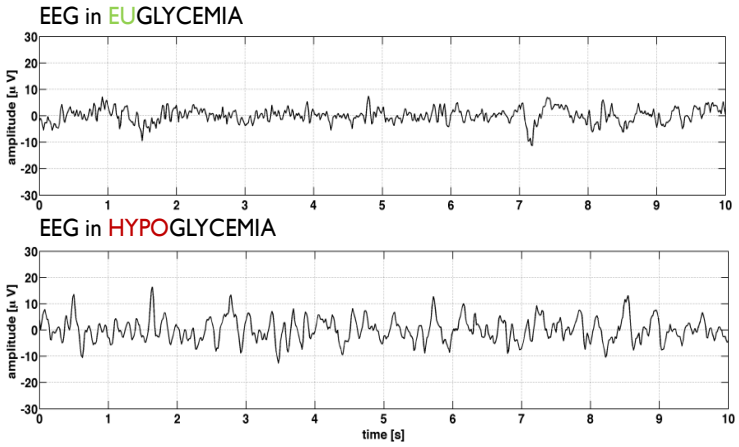


FIGURE 1.7: EEG signal during euglycemia (upper panel) and hypoglycemia (lower panel). Reproduced from [24].

Given that symptom perception as an estimation of the blood glucose level can be unreliable, as alternative or, more likely, complement to blood glucose sensors, the use of the EEG signal has been suggested to detect the entering in hypoglycemia. A research prototype portable device, able to measure the EEG signal by subcutaneous electrodes and then analyze and classify it in real-time, has been proposed for the detection of hypoglycemia-events [32]. This device proposed by Hyposafe was designed to

detect and alert T1D patients of hypoglycemia before the situation becomes critical by continuous measurement of the electrical activity within the brain (via EEG) [33]. This technology, patented in [34], is made by a 5 cm long, 0.5 mm diameter electrode implanted only a few millimeters below the skin, and a non-implanted device which stores and processes the EEG signal and contains a power source (18 h), a sound generator and a light indicator to inform the user of critical events, Fig. 1.8. Thus, Hyposafe idea is based on using the brain directly as a biosensor, measuring changes in EEG signals and monitoring for signs of hypoglycemia. The device can remain implanted for more than 10 years without creating inconvenience to the user. Moreover, there is no risk of infection or allergic reactions, because there are not physical elements passing through the skin and the use of bandage/plaster is not required [33].

The clinical studies of continuous EEG recording and real-time data processing during insulin-induced hypoglycemia in T1D patients conducted so far indicate that it might be possible to predict incidents of severe hypoglycemia before the patients are severely cognitive impaired both during daytime and sleep, [33] [35] [36]. Despite several contributions, a systematic evaluation of the effects of hypoglycemia in the brain to identify solid indicators sensitive to hypoglycemia has not been reported yet.

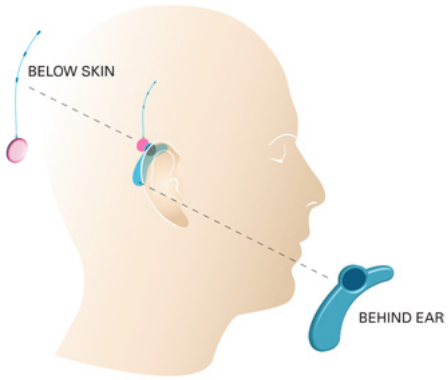


FIGURE 1.8: Technology made by a 5 cm long, 0.5 mm diameter electrode implanted only a few millimeters below the skin, and a non-implanted device which stores and processes the EEG signal and contains a power source (18 h), a sound generator and a light indicator to inform the user of critical events. Reproduced from [33].

## 1.3 Aim of the work

Starting from the findings in the literature, the main aim of this work is to identify potential margins of improvement in EEG processing and further features indicators sensitive to hypoglycemia to deepen the knowledge on the effects of hypoglycemia in the brain. So far, studies in the literature have mainly evaluated these changes only on a single EEG channel level on the frequency domain, but limited information is available on the hypoglycemia influence on brain network dynamics and on connection between brain different areas. After testing the well-known effect of hypoglycemia in the spectral power in all the 19 EEG channels, a multivariate analysis is applied (Chapter 3) to deepen the knowledge on hypoglycemia effects on EEG connectivity. Then, nonlinear indices originally developed for the

representation of chaotic systems are implemented to provide information complementary to that obtained by linear methodologies with a possible improvement of the hypoglycemia detection (Chapter 4). Furthermore, the different topographical configurations of electric potentials over the multichannel electrode array are evaluated both in euglycemia and hypoglycemia to investigate the changes in brain network dynamics (Chapter 5). Eventually, the interaction between all the quantitative EEG measures proposed and the results of behavioral tests are compared to research the important role of EEG quantitative changes in neurocognitive functions (Chapter 6). All these methodologies are tested on a database of T1D subjects who underwent an 8-h hyperinsulinemic-hypogycemic clamp experiment with the general goal of having a more complete overview on the effects of hypoglycemia in the brain.

# Chapter 2

# Database

Thirty-one patients [1] with T1D underwent an hyperinsulinemic – hypoglycemic clamp (described in Section 2.2) with a target of $2.0 - 2.5\ \mathrm{mmol\,l^{-1}}$. Nineteen patients (58 % males; mean age, $55 \pm 2.5$ years; diabetes duration, $28.5 \pm 2.5$ years) were recruited from the diabetes outpatient clinics at Nordsjællands Hospital Hillerød and Steno Diabetes Center, Denmark, while twelve patients (67 % males; mean age, $37.5 \pm 3.5$ years; diabetes duration, $15 \pm 3$ years) were recruited from the diabetes outpatient clinics at Hvidovre Hospital, Denmark. For further details, see Table 2.1. The database was kindly provided by Dr Claus B. Juhl, Dr Anne-Sophie Sejling, and Dr Christian Frandsen. Hyposafe A/S, Lynge, Denmark, assisted with providing the data.

## 2.1 Inclusion criteria

Inclusion criteria were type 1 diabetes for >3 years, age >18 years, and being either hypoglycemia aware or unaware. Exclusion criteria included pregnancy; breastfeeding; any brain disorder; use of antiepileptic drugs, $\beta$-blocking drugs, or neuroleptic drugs; use of benzodiazepines within the last month; cardiovascular disease; and alcohol or drug abuse. Hypoglycemia awareness

[1] The study was approved by the local ethical committee and the patients gave written informed consent.

TABLE 2.1: Database

| # | Patient ID | Awareness status | Gender | Age (y) | Diabetes duration (y) |
|---|---|---|---|---|---|
| 1) | 1 | Unaware | Female | 68 | 33 |
| 2) | 2 | Unaware | Male | 65 | 38 |
| 3) | 3 | Aware | Male | 45 | 15 |
| 4) | 6 | Aware | Male | 56 | 28 |
| 5) | 8 | Unaware | Male | 60 | 15 |
| 6) | 9 | Aware | Female | 66 | 33 |
| 7) | 10 | Unaware | Male | 62 | 37 |
| 8) | 11 | Unaware | Male | 55 | 35 |
| 9) | 12 | Aware | Female | 45 | 11 |
| 10) | 13 | Unaware | Female | 69 | 45 |
| 11) | 15 | Aware | Male | 42 | 16 |
| 12) | 16 | Unaware | Male | 59 | 20 |
| 13) | 19 | Unaware | Female | 52 | 34 |
| 14) | 20 | Unaware | Male | 67 | 23 |
| 15) | 21 | Aware | Male | 36 | 18 |
| 16) | 23 | Unaware | Female | 53 | 33 |
| 17) | 24 | Unaware | Female | 45 | 27 |
| 18) | 26 | Unaware | Male | 66 | 54 |
| 19) | 27 | Unaware | Female | 40 | 27 |
| 20) | D6 | Aware | Female | 42 | 18 |
| 21) | D9 | Aware | Male | 51 | 14 |
| 22) | D12 | Aware | Male | 38 | 8 |
| 23) | D15 | Aware | Male | 29 | 15 |
| 24) | D18 | Reduced awareness | Male | 40 | 20 |
| 25) | D20 | Aware | Female | 36 | 22 |
| 26) | D21 | Aware | Male | 22 | 7 |
| 27) | D26 | Aware | Male | 66 | 37 |
| 28) | D28 | Aware | Male | 28 | 16 |
| 29) | D33 | Aware | Female | 26 | 20 |
| 30) | D34 | Reduced awareness | Male | 29 | 15 |
| 31) | D40 | Reduced awareness | Female | 43 | 3 |

status was classified by the Pedersen-Bjergaard method [37], the Gold score [38], and the Clarke method [39]. Of the 31 participants, 13 patients were classified as hypoglycemia unaware and 15 patients as hypoglycemia aware according to all three methods, while 3 patients as hypoglycemia unaware according to two methods (labeled with *reduced awareness* in Tab. 2.1). Patients who did not qualify as either hypoglycemia aware or unaware were excluded from the analyses.

## 2.2 Experimental protocol

For the clamp procedure, insulin (Actrapid; Novo Nordisk, Ballerup, Denmark) mixed with heparinized plasma from the patient and isotonic saline was administered intravenously at a rate of 1 mU insulin/kg/min for the progressive induction of hypoglycemia. A variable 20% glucose infusion was administered to keep plasma glucose at the desired levels. During the experiment lasting about 8 hours, blood glucose (BG) samples monitored (Yellow Springs Inc (YSI), USA) every 5 minutes to individualize at least 1-h of hypoglycemia (HYPO) and 1-h of euglycemia (EU) and 19 EEG channels were simultaneously recorded (Cadwell, Easy II, Kennewick, USA) using standard cap electrodes placed on the scalp according to the international 10/20 system, while the patients were sitting in a chair with eyes open. Offline, EEG was analogically low-pass filtered to avoid aliasing, then digitally acquired and finally down-sampled at 200 Hz. The dynamic range of the EEG was $\pm 4620\ \mu V$ with an amplitude resolution of $0.14\ \mu V$. The internal noise level in the analogue data acquisition system was estimated to be $1.3\ \mu V$ RMS. In Fig. 2.1, P3-A1A2 EEG channel recording and simultaneous BG data from a representative subject are visible. 1-h of EU and 1-h of HYPO and 1-h of recovery after induced-hypoglycemia were individualized by visual

inspection of the BG time-series before and after it crossed the hypoglycemic threshold of 70 mg/dL.

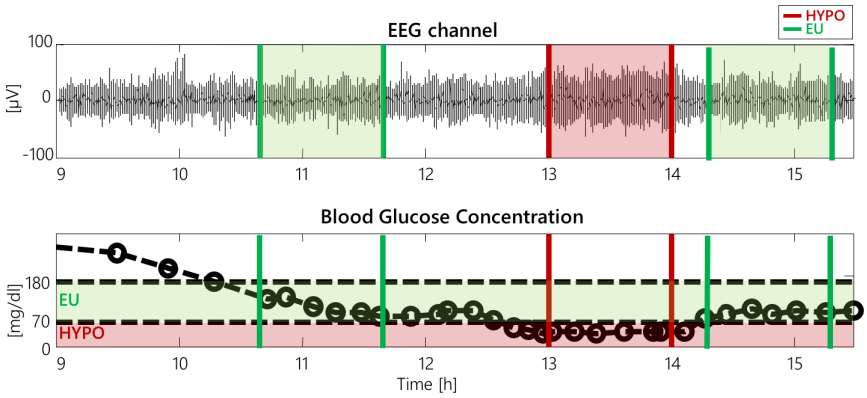


FIGURE 2.1: Data from a representative subject during the hyperinsulinemic-hypoglycemic clamp. On the upper panel, P3-A1A2 electroencephalography (EEG) recordings and on the lower panel, simultaneous blood glucose concentration (open circles denote reference YSI samples and the dashed line denotes their spline interpolation). Vertical green and red lines refer to 1-h EU- and HYPO-glycemic and Recovery intervals.

Furthermore, two different cognitive tests were performed in EU (pre and post induced-hypoglycemia) and HYPO: Trail 5 B of the Comprehensive Trail Making Test (TMT B) and the Stroop tests.

## 2.3 Behavioral tests

### 2.3.1 Trail Making Test

The Trail Making Test is a neuropsychological test of motor speed and visual attention composed by two parts. In part A, i.e., TMT A, the subject's task is to quickly draw lines on a page connecting

TABLE 2.2: TMT B

| Group Age [years] | Score [s] |
|---|---|
| 25-34 | $50.68 \pm 12.36$ |
| 35-44 | $58.46 \pm 16.41$ |
| 45-54 | $63.76 \pm 14.42$ |
| 55-59 | $68.74 \pm 21.02$ |

25 consecutive numbers without lifting the pen from the paper. If the patient makes an error, it is pointed out immediately and it is allowed the patient to correct it. The performance is assessed by the time taken to complete the trial correctly. In part B, i.e., TMT B, it is tested how fast the participant can connect numbers and letters in alternating increasing sequence (i.e., 1-A-2-B, etc.). TMT B is 56 cm longer and has more visually interfering stimuli than TMT A. Part B is more difficult than Part A not only because it is a more difficult cognitive task, but also because of its increased demands in motor speed and visual search [40]. Thus, TMT B evaluates visual attention, motor speed, and cognitive alternation. In Tab 2.2, an example from [41] of the mean time necessary to complete TMT B stratified by age is reported.

### 2.3.2 Stroop test

The Stroop tests evaluate processing speed and selective attention. Specifically, in the Danish version of the Stroop Color and Word Test by Golden [42], the participant must name as many items as possible in 45 s at three different conditions: color names printed in black (Stroop word), blocks printed in different colors (Stroop color), and color names printed in non-matching colors (Stroop combi) [43]. The Stroop test proved how the brain

slows down if it has to deal with conflict information. For instance, to complete the last task is more challenging than the first ones because of the brain processing delay caused by the interfering information of color names printed in non-matching color. Moreover, the more the capacity to direct attention is fatigued, the harder this last stage becomes. In Fig. 2.2, the effect of interfering word stimuli upon naming colors serially is reported as the mean time for a group of one hundred students (results reproduced from one of the original studies of J. Ridley Stroop [44]).

TABLE III

THE MEAN TIME FOR NAMING ONE HUNDRED COLORS PRESENTED IN SQUARES AND IN THE PRINT OF WORDS WHICH NAME OTHER COLORS

| Sex | No. Ss. | *NCWd* | $\sigma$ | *NC* | $\sigma$ | *D/NC* | *D* | $PE_d$ | $D/PE_d$ |
|---|---|---|---|---|---|---|---|---|---|
| Male..... | 29 | 111.1 | 21.6 | 69.2 | 10.8 | .61 | 42.9 | 3.00 | 13.83 |
| Female..... | 71 | 107.5 | 17.3 | 61.0 | 10.5 | .76 | 46.5 | 1.62 | 28.81 |
| Male and Female..... | 100 | 110.3 | 18.8 | 63.3 | 10.8 | .74 | 47.0 | 1.50 | 31.38 |

FIGURE 2.2: The means of the times for the NC (Naming colors) and NCWd ( Naming the Colors of the Print of Words Where the Color of the Print and the Word are Different) tests for a group of 100 students and for each sex are presented with the difference, the probable error of the difference, the reliability of the difference, and difference divided by the mean time for the naming color test. Reproduced from [44].

# Chapter 3

# Frequency domain features

## 3.1 State of the art

An association between hypoglycemia and EEG changes has been proved in many works in the literature. Indeed, the EEG signal reflects the metabolic state of the brain during the critical state of hypoglycemia. In [45], authors provide a review of the current literature regarding changes in the EEG during episodes of low blood glucose. An increase in the total EEG power and a generalized slowing of the frequency are seen symmetrically in all cerebral regions and occur irrespective of age, diabetes duration, awareness status, or antecedent episodes of hypoglycemia. More specifically, an increase during hypoglycemia in both the power of theta and alpha band is indicated in [46] [47] [48] [49] [50]. Moreover, the centroid frequency (CF) of theta band is often increased, while the CF of alpha band is reduced [51]. These changes (summarized in Tab. 3.1) in EEG signals can be qualitatively appreciated by visual inspection of the representative data in Fig. 3.1, in which 5-s segments measured in EU are shown with those recorded in the same subject when he or she is exposed to HYPO. At the single-channel level, EEG in HYPO (Fig. 3.1 D and G) shows higher amplitudes in the low-frequency bands and greater regularity than the one in EU (Fig. 3.1 C and F). While assessing the synchronization of pairs of EEG sweeps in the same

TABLE 3.1: Overview of studies investigating hypoglycemia EEG changes in the last decade

| **Study** | **Year** | **N** | $\frac{aware}{unaware}$ | $Power_{theta}$ | $CF_{theta}$ | $Power_{alpha}$ | $CF_{alpha}$ |
|---|---|---|---|---|---|---|---|
| [46] | 2016 | 8 | nd | $\uparrow$ | $\rightarrow$ | $\uparrow$ | $\downarrow$ |
| [47] | 2016 | 19 | nd | $\uparrow$ | $\uparrow$ | $\uparrow$ | $\rightarrow$ |
| [22] | 2015 | 23 | $\frac{9}{14}$ | $\uparrow$ | $\rightarrow$ | $\rightarrow$ | $\rightarrow$ |
| [48] | 2014 | 19 | nd | $\uparrow$ | $\uparrow$ | $\uparrow$ | $\rightarrow$ |
| [52] | 2013 | 5 | nd | $\downarrow$ | $\uparrow$ | $\uparrow$ | $\downarrow$ |
| [49] | 2013 | 9 | $\frac{3}{6}$ | $\uparrow$ | nd | $\uparrow$ | nd |
| [50] | 2012 | 35 | $\frac{6}{28}$ | $\uparrow$ | $\rightarrow$ | $\uparrow$ | $\downarrow$ |
| [53] | 2010 | 6 | nd | $\rightarrow$ | $\uparrow$ | $\rightarrow$ | $\downarrow$ |
| [30] | 1996 | 14 | $\frac{7}{7}$ | $\uparrow$ | $\uparrow$ | $\downarrow$ | $\downarrow$ |
| [51] | 1996 | 14 | $\frac{7}{7}$ | $\uparrow$ | nd | $\downarrow$ | $\downarrow$ |
| | | | | $\uparrow$ increase in HYPO; | $\downarrow$ decrease in HYPO; | $\rightarrow$ no change; | $nd$ not determined |

glycemic condition by visual inspection is challenging, calling for the use of multivariate analysis tools.

Although the notion that hypoglycemia affects EEG rhythms is well established, limited information is available on if and how hypoglycemia influences the connectivity between different brain areas. To the best of our knowledge, existing publications have focused on univariate EEG studies and in [54], connectivity was assessed with phase coherence [55], phase lag index [56], synchronization likelihood [57], and phase slope index [58] showing a decline in patients with T1DM ($N = 119$) respect to controls ($N = 61$), but it was not shown what happens in HYPO respect to EU. Over the last twenty years, a lot of parametric and non-parametric connectivity methods describing the interactions between cortical areas by the direction and the strength of the information flow have been proposed [59] [60], and their performance compared [61] [62]. Here, after reporting the changes in the power and centroid frequency in all T1D patients, we used a

multivariate approach called information partial directed coherence (iPDC) to quantify the functional connectivity between EEG channel-pairs in EU and HYPO conditions. In particular, iPDC is computed through the use of multivariate autoregressive (MAR) models of T3-A1A2, T4-A1A2, T5-A1A2, T6- A1A2, P3-A1A2, P4-A1A2, Pz-A1A2, C3-A1A2, C4-A1A2, Cz-A1A2, O1-A1A2, and O2-A1A2 EEG channels recordings in 19 T1D subjects. The value of iPDC in both the theta and alpha bands was examined when passing from EU to HYPO.

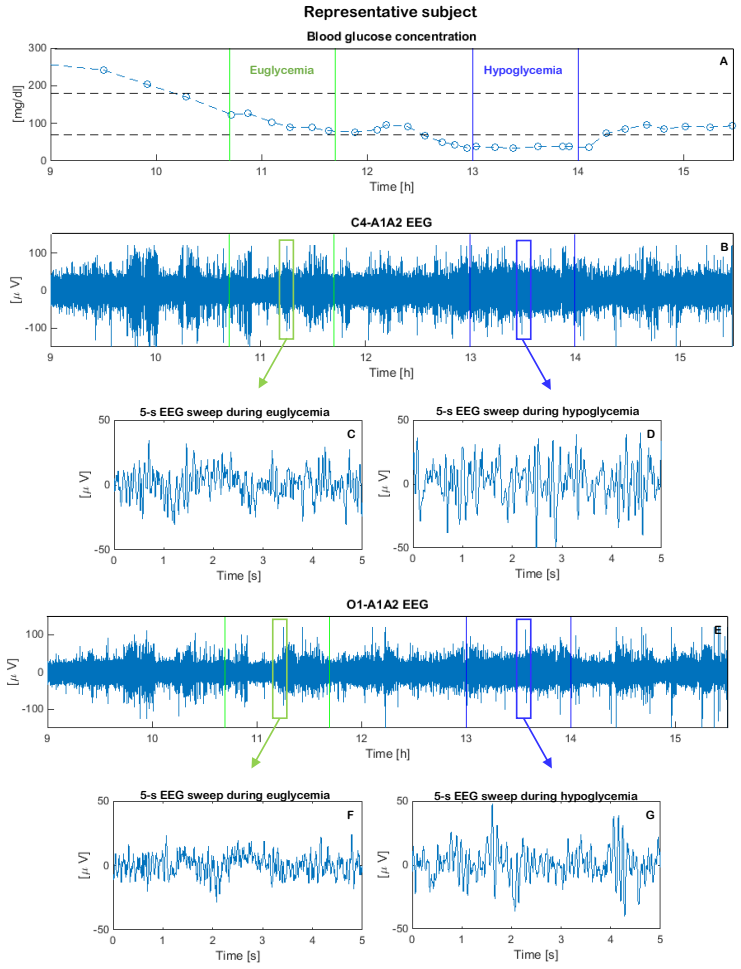


FIGURE 3.1: Data from a representative subject during the hyperinsulinemic-hypoglycemic clamp: (A) blood glucose concentration (open circles denote reference YSI samples; the dashed lines denote their spline interpolation) and simultaneous raw (B) C4-A1A2 and (E) O1-A1A2 electroencephalography (EEG) recordings. Vertical green and blue lines refer to 1-h EU and HYPOglycemic intervals, respectively. For each glycemic condition, 5-s EEG sweeps are shown (C and D) for C4-A1A2 and (F and G) for O1-A1A2, where t = 0 is the sweep start time.

## 3.2 Methods

### 3.2.1 EEG spectral power

A frequency analysis was performed for 5-min EU and HYPO intervals, using a Welch's power spectral density (PSD) in delta ([1-3.4] Hz), theta band ([4.8-7] Hz), alpha ([9-12] Hz) and beta ([14-17] Hz) frequency bands. In particular, PSD was found using Welch's overlapped segment averaging estimator: the signal is divided in 4-s sections to obtain segments 50% overlapped. Each segment is windowed with a Hamming window. Then, the segments periodograms are averaged to obtain the PSD estimation. Then, both absolute and relative power in all four frequency bands were estimated from the averaged PSD. In particular, relative power was obtained by diving the absolute power in each band by the total power in the range [1-40] Hz. Thus, for each subject two vectors (1 x 19) containing the power for each EEG channel in not overlapping delta, theta, alpha, and beta bands were obtained in both EU and HYPO conditions. Eventually, to assess for each subject and each channel, whether or not the changes in the absolute and relative power value were statistically significant when passing from EU to HYPO, paired Student's t-tests were computed under the hypothesis of normal distribution of samples (Lilliefors test) otherwise, Wilcoxon rank-sign tests were considered (a value of $p < 0.05$ was considered significant).

### 3.2.2 EEG centroid frequency

For each 5-min EU and HYPO intervals, the CF, i.e., the center of gravity of each frequency band that subdivides the area under the spectral curve into two of equal size, was also computed. In particular, the CF was calculated in each band, i.e., delta, theta,

alpha and beta, and it was assessed for each subject and each channel, if or not the CF value were statistically significant when passing from EU to HYPO, paired Student's t-tests were computed under the hypothesis of normal distribution of samples (Lilliefors test) otherwise, Wilcoxon rank-sign tests were considered (a value of $p < 0.05$ was considered significant).

### 3.2.3 EEG-based functional connectivity

The functional organization of the brain is characterized by segregation and integration of information being optimally processed. Functional interactions seem to be provided by synchronized activity, both locally and between distant brain regions. Brain networks thus consist of spatially distributed but functionally connected regions that process information [63]. In such a context, functional connectivity (FC) is defined as the temporal dependency of neuronal activation patterns of anatomically separated brain regions. FC reflects statistical dependencies between distinct and distant regions of information processing neuronal populations [63]. In the multivariate analysis of biomedical signals, especially for EEG, several methods have been proposed to evaluate FC [64] [59], for example through computing cross-correlations in the time or frequency domain, mutual information or spectral coherence. FC captures patterns of statistical dependence [65], but it is well known that statistical dependency is a necessary yet not sufficient condition for causality [66]. Granger causality is a widely used data-driven approach to assess the connectivity among different brain regions and to determine the directional causal interaction among EEG signals [67]. Several variants of Granger causality have recently been applied to neurophysiological data to gain insight in the direction of influences between neural systems [68].

**Information Partial Directed Coherence (iPDC)**

In this chapter, we chose iPDC to evaluate the mutual relation between the EEG channels for three main reasons.

1. Estimates of connectivity based on MAR models are robust to the high contribution of noise in EEG signals.

2. iPDC, in contrast to coherence, considers if the dependence from two signals comes from the influence of a third one which drives them.

3. Eventually, iPDC allows assessing directionality.

The iPDC has been recently presented by Takahashi et al [69], as an improvement of partial directed coherence [68] and general partial directed coherence [70]. Indeed, iPDC is considered more stable than other approaches in FC assessment when signals have large differences in their amplitudes, as happens with EEG in hypoglycemia compared with EEG in euglycemia in our case study. iPDC is a multivariate spectral measure to compute the directed influences between any given pair of signals (i,j) of a multivariate dataset. This information is condensed in a complex function $iPDC_{i\leftarrow j}(f)$ of the frequency $f$, which measures the relative interaction of the signal $j$ with regard to signal $i$ as compared with interactions of all $j$'s with other signals in the multivariate dataset. Although we refer the reader to Takahashi et al [69] for the mathematical details, the following two steps briefly describe the procedure for computing iPDC.

In the first step, an MAR model is identified by fitting it against EEG data streams acquired from $L$ different channels. Formally, letting $x(n)$ :

$$x(n) = [x_1(n), x_2(n), ..., x_L(n)]^T \;\; n = 1, 2, ..., N \tag{3.1}$$

(where T stands for transpose) be the vector containing the samples at the n-th sampling instant $n$ ($n = 1, ...N$) of the $L$ considered EEG channels $x_1, x_2, ..., x_L$, the MAR model of order $p$ is described as:

$$x(n) = -\sum_{r=1}^{p} A_r x(n-r) + w(n) \tag{3.2}$$

where $A_r \;\; r = (1, ..., p)$ are $LxL$ unknown matrices of model coefficients, and the $L$-size column vector $w(n)$ is the innovation process with covariance matrix $\Sigma_W$ [69]. The matrices $A_r \;\; r = (1, ..., p)$ and $\Sigma_W$ are estimated by least squares exploiting the so-called Yule–Walker equations [71]:

$$\begin{bmatrix} R_{xx}(0) & R_{xx}(-1) & \cdots & R_{xx}(-p+1) \\ R_{xx}(1) & R_{xx}(0) & & R_{xx}(-p+2) \\ \vdots & & \ddots & \vdots \\ R_{xx}(p-1) & R_{xx}(p-2) & \cdots & R_{xx}(0) \end{bmatrix} \begin{bmatrix} A_1^T \\ A_2^T \\ \vdots \\ A_p^T \end{bmatrix} = - \begin{bmatrix} R_{xx}(1) \\ R_{xx}(2) \\ \vdots \\ R_{xx}(p) \end{bmatrix} \tag{3.3}$$

where the $R_{xx}(k)$ matrices are the covariance matrices computed from the available EEG data as

$$R_{xx}(k) = \begin{cases} \frac{1}{N} \sum_{n=0}^{N-1-k} x(n) x^T(n+k) & k = 0, 1, ..., N-1 \\ \frac{1}{N} \sum_{n=-k}^{N-1} x(n) x^T(n+k) & k = -(N-1), -(N-2), ..., -1 \end{cases} \tag{3.4}$$

In Eq. 3.2 model order $p$ is found by trail until the Akaike information criterion (AIC) index

$$AIC(p) = N \ln |\Sigma_W| + 2L^2 p \tag{3.5}$$

(where $|\,|$ denotes the matrix determinant) is minimized [72].
In the second step, having defined the complex matrix $B(f)$ as

$$B(f) = I_L - \sum_{r=1}^{p} A_r e^{-j2\pi f} \tag{3.6}$$

where $I_L$ is the identity matrix and $j$ is the imaginary unit in this equation, the iPDC complex function from the time-series $j$ to the time-series $i$ is obtained by

$$iPDC_{i \leftarrow j}(f) = \sigma_{W_u}^{-1/2} \frac{b_{ij}(f)}{\sqrt{b_j^H(f) \Sigma_W^{-1} b_j(f)}} \tag{3.7}$$

where $b_j(f)$ and $b_{ij}(f)$ are, respectively, the $j$-th column and the $(j,i)$-th element of matrix $B(f)$, $\sigma_{W_u}$ is the $(i,i)$-th element of the innovation covariance matrix $\Sigma_W$, and the apex $H$ in $b_j^H$ stands for the Hermitian transpose (i.e., obtained from $b_j$ by taking the transpose and then the complex conjugate of its components). The complex function $iPDC_{i \leftarrow j}(f)$ of Eq. 3.7 is usually analyzed in terms of its absolute value [69].

### iPDC computation

The analysis was applied to 15 min of the EU and HYPO intervals [1]. $L = 12$ EEG channels were considered, and each 15-min interval of EU and HYPO was divided in 5-s sweeps, resulting in $N = 1000$ samples per sweep, a quantity sufficient to obtain stable results according to Florin et al [73]. At the same time, 5-s intervals are narrow enough to invoke pseudo-stationarity assumptions on EEG (e.g., as done by Abásolo et al [74] ). For each sweep, an MAR model as in Eq. 3.2 was identified. Regarding the model order $p$, we first considered, for each sweep, the value minimizing $AIC(p)$ of Eq. 3.5 among candidate orders ranging from 1 to 20; then, among the estimated values of $p$, we chose the

[1] This analysis was applied to the first 19 T1D patients of Tab. 2.1, because only these data were available when this method was implemented.

highest and used it as the model order for all sweeps under analysis for a given subject (the resulting $p$ was always 9 or 10). The rationale behind this decision is that, to detect coupling directions in multivariate oscillatory systems, the MAR model should have a high order [75], and at the same time, overestimating the model order is better than underestimating it [73]. Then, for any pair $(i, j)$, the function $iPDC_{i \leftarrow j}(f)$ of Eq. 3.7 was computed in theta ([4–8] Hz) and alpha ([8–13] Hz) bands for each sweep. Eventually, the absolute mean profiles $iPDC_{i \leftarrow j}(f)$, referred to the whole interval of 15 min, were computed by averaging the absolute values of the $iPDC_{i \leftarrow j}(f)$ profiles estimated in the 5-s sweeps (throughout this chapter, for sake of brevity, the symbol $\overline{iPDC}$ will be used without explicitly showing the dependence on frequency and channel pair).

**iPDC values analysis**

Because the values of $\overline{iPDC}$ can be pretty low, it is necessary, before evaluating changes passing from EU to HYPO, to determine an analytical threshold exploiting surrogate data. In particular, 15-min surrogate data in EU and HYPO were obtained randomly changing the time order of a set of real data (i.e., randomly permuting in temporal order the samples of the original series and so maintaining mean, variance, and histogram distribution of the original data) [76]. Then, as for real data, iPDC was estimated, and two thresholds for EU and HYPO, respectively, were calculated as 5% of the absolute value of $\overline{iPDC}$ [77]. Thus, before applying the statistical tests to evaluate if there were remarkable changes passing from EU to HYPO, it was checked if $\overline{iPDC}$ results were above the threshold estimated at any frequency. Eventually, to assess for each subject whether or not the changes in the absolute value of $\overline{iPDC}$ were statistically significant when

passing from EU to HYPO, paired Student's t tests were computed under the hypothesis of normal distribution of samples (Lilliefors test); otherwise, Wilcoxon rank-sign tests were considered (a value of $p < 0.05$ was considered significant). After that, for each subject, the average value of $\overline{iPDC}$ was computed to obtain a scalar indicator for the EU and HYPO intervals. This scalar indicator (which subsequently in this chapter will be denoted by the symbol $\overline{\overline{iPDC}}$) is obviously much simpler to handle than the function $\overline{iPDC}$ for the analysis.

## 3.3 Implementation

### 3.3.1 Preprocessing

As far as the analyses of the EEG power and the CF, for each subject, a pre-analysis was developed considering, in each subject, two intervals referred to as EU and HYPO, respectively, targeted from the available BG data. In particular, for each subject, two 1-h intervals corresponding to EU and HYPO conditions, respectively, were identified from the BG time-series by visual inspection detecting when the glycemic thresholds at 70 and 180 mg/dL were crossed by a smoothing spline approximation of the samples. Then, 5-min intervals in both EU ([70-180] mg/dL) and HYPO (<70 mg/dL) conditions were selected. EEG data in EU and HYPO were band-pass filtered between 1 and 40 Hz using a 4-order Butterworth filter; Independent Component Analysis was applied in order to remove cardiac and oculomotor artifacts (only components with clear eye blinks, saccades and cardiac artefacts were excluded). EEG signals were re-referenced to the common average-reference.

Concerning the iPDC analysis, as previously described, only EEG channels in the temporal, central, parietal, and occipital lobes

(i.e., the L=12 EEG time-series referred to, respectively, as the T3-A1A2, T4-A1A2, T5-A1A2, T6-A1A2, P3-A1A2, P4-A1A2, Pz-A1A2, C3-A1A2, C4-A1A2, Cz-A1A2, O1-A1A2, and O2-A1A2 channels) were considered because their analysis is simplified from the virtual absence of artifacts (e.g., eye-induced, muscle activation-induced). EEG data were not band-pass-filtered before computing iPDC in order to avoid possible distortions in the results [73]. A pre-analysis selected by visual inspection 15-min intervals in both EU ([70-180] mg/dL) and HYPO (<70 mg/dL) conditions from BG time series (smoothed by a spline approximation of the samples).

## 3.4 Results

### 3.4.1 Power spectra results

Representative randomly chosen 1-s EEG sweeps are depicted in Fig. 3.2 to appreciate in all channels, albeit qualitatively, differences of the EEG signal in EU (in panel (a)) and HYPO (in panel (b)). As apparent as in Fig. 3.1, the EEG in HYPO shows higher amplitudes in the low frequency bands and greater regularity than the one in EU.

As far as the frequency-domain analysis is concerned, the average relative power in theta (Fig. 3.2 panel (d)) band confirms the higher amplitude of low-frequency EEG rhythms during hypoglycemia with respect to euglycemia in all electrodes ($p < 0.0263$). Actually, considering the whole population of subjects, the relative power in alpha (Fig. 3.2 panel (e)) band shows a statistically significant increase when passing from EU to HYPO in parietal and occipital lobes ($p < 0.0023$). Eventually, a significant decrease is seen in beta band in all electrodes ($p < 0.0357$). While, there were not significant differences in delta band.

### 3.4.2 Centroid frequency results

In line with the reported results in the literature, the CF tends to decrease in the alpha band [51]. In particular, a statistically significant slowing of the CF during HYPO respect to EU was found in T4-A1A2 ($p = 0.03$), T6-A1A2 ($p = 0.02$), and O1-A1A2 ($p = 0.02$) in alpha band. In Fig. 3.3, the boxplots for the CF values in the above cited EEG channels are reported.

### 3.4.3 iPDC results

The absolute values of the iPDC function $iPDC_{i\leftarrow j}(f)$ computed in two 5-s representative sweeps are shown in Fig. 3.4 for a representative participant in both the theta (left panel) and alpha (right panel) bands before (thin upper line) and after entering in hypoglycemia (thick lower line). The absolute values of iPDC are rather low but above the computed thresholds (dashed lines) that indicate the minimal level of iPDC considered as null. Remarkably, a very visible change passing from EU to HYPO can be observed in both bands. All the other sweeps referred to this participant showed iPDC profiles for all combinations of channels qualitatively similar to those of Fig. 3.4. The same, on average, happens in the entire database of subjects.

Considering the function $\overline{iPDC}$ , it tends to decrease when passing from EU to HYPO in both theta and alpha bands in all combinations of the considered EEG channels. An example of results is documented in Fig. 3.5, which displays, for the representative subject, $\overline{iPDC}$ from T5-A1A2 to C3-A1A2 and from O1-A1A2 to C4-A1A2 in the theta band (left panels) and from O1-A1A2 to T4-A1A2 and from O1-A1A2 to C4-A1A2 in the alpha band (right panels) in EU (thin upper line) and HYPO (thick lower line). Considering the entire dataset, in the theta band the

function $\overline{iPDC}$ significantly decreases ($p < 0.01$) in 17 of 19 subjects from T5-A1A2 to C3-A1A2, from O1-A1A2 to C4-A1A2, and from O2-A1A2 to Cz-A1A2. In the alpha band it significantly decreases ($p < 0.01$) in 17 of 19 subjects from O1-A1A2 to T4-A1A2 and from O1-A1A2 to C4- A1A2.

In Fig. 3.6 we report a boxplot of the values, obtained from the entire pool of subjects, of the scalar indicator $\overline{\overline{iPDC}}$ for the eu and hypoglycemic intervals. In particular, $\overline{\overline{iPDC}}$ from O1-A1A2 to C4-A1A2 tends to decrease ($p < 0.01$) passing from EU to HYPO, and its variability tends to decrease passing from EU to HYPO.

Because of $\overline{\overline{iPDC}}$ changes in HYPO, it is interesting to assess, albeit in a preliminary fashion, the potential discriminatory power of a classifier driven by $\overline{\overline{iPDC}}$. To do so, we exploited $\overline{\overline{iPDC}}$ from O1-A1A2 to C4-A1A2 related to the 17 subjects in whom $\overline{\overline{iPDC}}$ significantly decreased passing from EU to HYPO. These values were used to train a support vector machine classifier (with a gaussian radial basis function kernel with a scaling factor of 1.108). In particular, using the leaving-one-out approach, 16 out of 17 observations were used as the validation set, and the remaining observation was used as the training set (each observation includes $\overline{\overline{iPDC}}$ in both the theta and alpha bands for each subject). This step is repeated on all ways to cut the original sample.

Classification resulted in 12 of 17 euglycemic events (true-negative rate) and in 13 of 17 hypoglycemic events (true-positive rate) correctly estimated, corresponding to a specificity of 71%, a sensitivity of 76%, and an accuracy of 74%. These classification results are in line, if not slightly better, than those reported in previous EEG studies in HYPO [78] [79]. Iaione and Marques [79] reported an overall accuracy rate of 71.3%, sensitivity of 71.1%,

and specificity of 71.5% in seven subjects during EU and spontaneous HYPO, and Nguyen et al [78] showed a sensitivity and specificity of 75% and 60%, respectively, in five T1D patients during an overnight clamp.

The classification performance from $\overline{\overline{iPDC}}$ resulted in a sensitivity and specificity higher than those obtained by us, on the same database, by applying univariate analysis exploiting the integral of the power spectral density, the integral of the logarithm of the squared power spectral density, the centroid frequency [50], and the reactivity index [80]. Both sensitivity and specificity in the hypodetection did not exceed 63%.

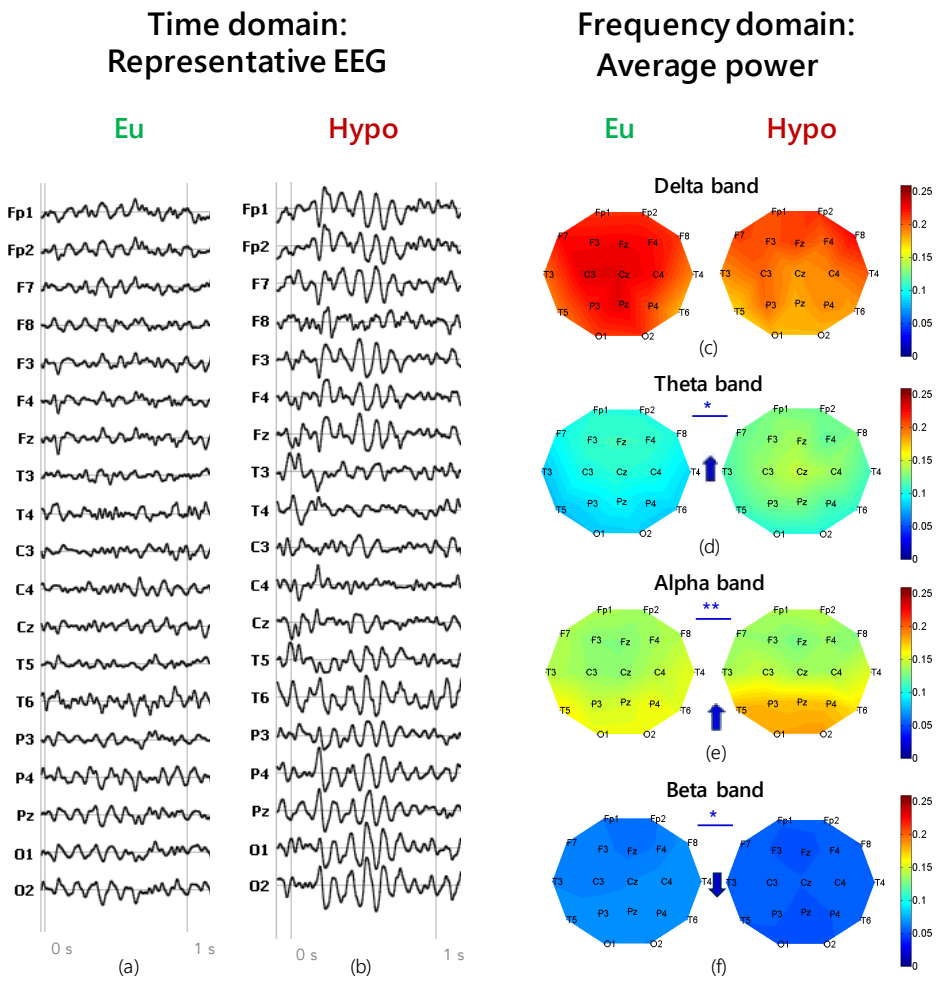


FIGURE 3.2: 1-s EEG signals during (a) EU and (b) HYPO in a representative subject and EEG relative spectral power topography in EU and HYPO averaged across all T1D patients in all frequency bands. During HYPO, there is: (c) not a significant power difference from EU in delta band [1-3.4] Hz; (d) a significant increase in theta band[4.8-7]Hz in all electrodes ($p < 0.0263$); (e) a significant increase in alpha band [9-12] Hz in parietal and occipital lobes ($p < 0.0023$); (f) a significant decrease in beta band [14-17] Hz in all electrodes ($p < 0.0357$).

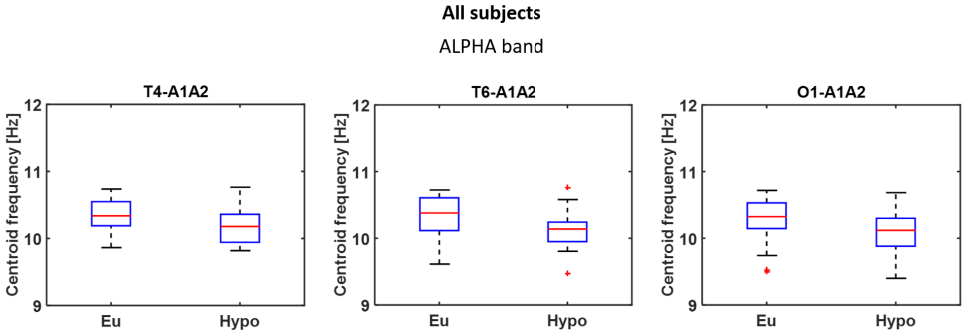


FIGURE 3.3: (From left to right) Centroid frequency in T4-A1A2 ($p = 0.03$), T6-A1A2 ($p = 0.02$), and O1-A1A2 ($p = 0.02$) in EU and HYPO in alpha band.

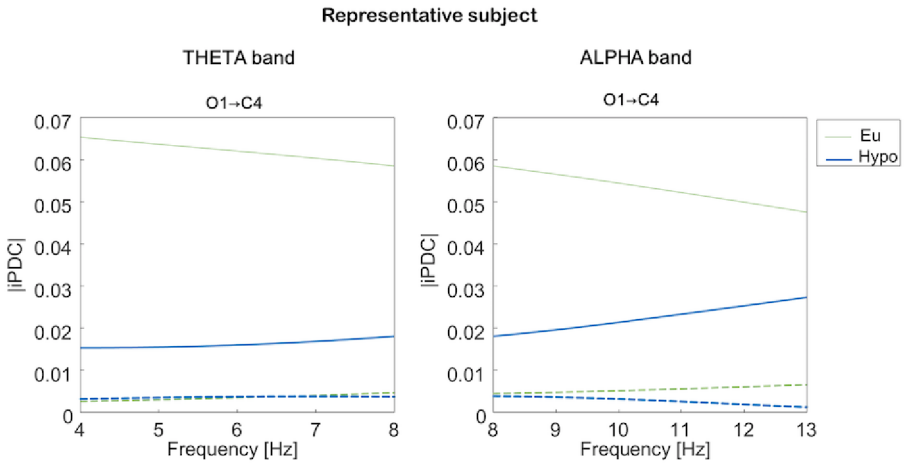


FIGURE 3.4: Information partial directed coherence (iPDC) in a representative subject. The absolute value of iPDC from O1- A1A2 to C4-A1A2 was computed from a randomly chosen 5-s sweep in the (left panel) theta and (right panel) alpha bands in EU (thin upper line) and HYPO (thick lower line).

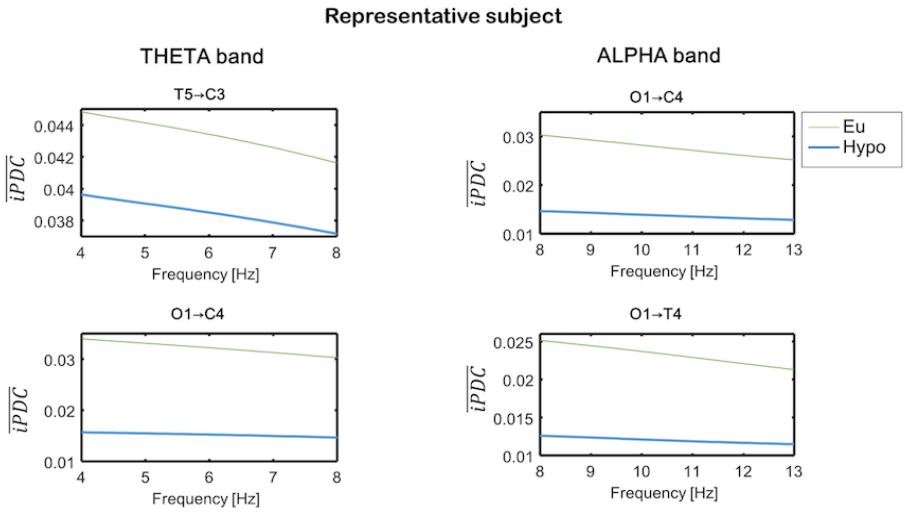


FIGURE 3.5: The information partial directed coherence function (iPDC) in a representative subject. The $\overline{iPDC}$ is estimated (left panels) from T5-A1A2 to C3-A1A2 and from O1-A1A2 to C4-A1A2 in the theta band and (right panels) from O1- A1A2 to C4-A1A2 and from O1-A1A2 to T4-A1A2 in the alpha band in EU (thin upper line) and HYPO (thick lower line).

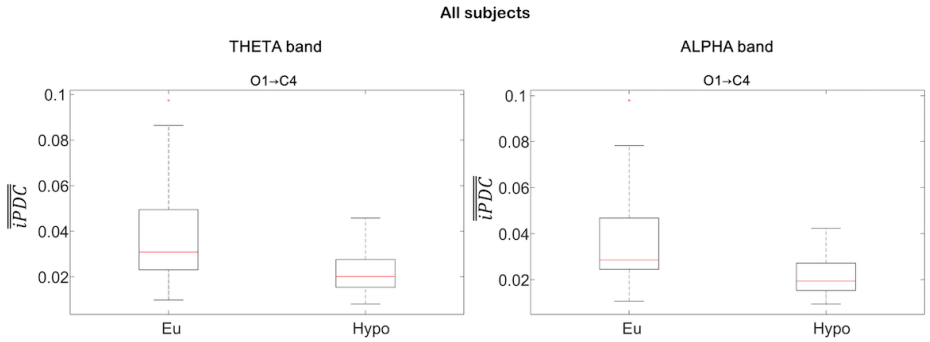


FIGURE 3.6: The scalar indicator of the information partial directed coherence function ($\overline{\overline{iPDC}}$) from the entire pool of subjects (n = 19). Box plots are shown of $\overline{\overline{iPDC}}$ from O1-A1A2 to C4-A1A2 in EU and HYPO in (left panel) theta and (right panel) alpha bands from all subjects. In each box the central line is the median value, the edges of the box are the 75th and 25th percentiles, the whiskers extend to the most extreme data points that are not outliers, and the crosses plotted individually stand for the outliers.

## 3.5 Discussion

In this chapter, we focused our attention on the effect of HYPO in the frequency domain. In particular, we found an overall increase of power in theta band and an occipital and parietal increase of power in alpha band compensated by a parallel overall decrease of power in beta band during HYPO respect to EU. The general slowing in alpha band was also confirmed by a statistically significant shifting of the centroid frequency during HYPO respect to EU. However, the changes induced by HYPO influenced also the results in the EEG functional connectivity. $\overline{iPDC}$ tended to decrease when passing from EU to HYPO in both theta and alpha bands in all combinations of the considered EEG channels. These preliminary findings corroborate the hypothesis that the altered cerebral activity caused by HYPO is reflected by a general slowing in the frequency domain.

# Chapter 4

# Analysis of complexity

## 4.1 State of the art

For the scope of detecting important dynamical properties of the physiological phenomena which are hidden in the EEG data during hypoglycemia, nonlinear methods can provide information complementary to that obtainable by linear methodologies, with a possible improvement of the performance. A particular problem of biological time series analysis comes from the fact that statistical characteristics can vary with time. Frequency domain parameters give assessment of the autonomic function, but the reliability of spectral power diminishes with the decrease in power signal and signal-to-noise ratio [81]. Many studies, e.g. [82], showed the decrease of EEG complexity in physio-pathological and impaired consciousness condition, proving the usefulness of complexity tools to increase the knowledge on these altered states. Applying nonlinear complexity indexes to analyze hypoglycemia-associated EEG changes might provide new insights into the effects of HYPO on the brain and support neurophysiologists in understanding more in depth the functioning of the brain during HYPO. However, to the best of our knowledge, application of nonlinear indicators to the specific problem includes only the investigation reported in [48], where a decrease of EEG *complexity* (here intended as irregularity) was shown to be induced

by hypoglycemia by computing the sample entropy index (Samp En) at various scale factors, employing the so-called multiscale entropy algorithm (MSE) [83]. While entropy-based algorithms are very popular and powerful for analyzing biomedical signals [84] [85] [86] [82] [87] [88] [89] [90] [91] [92] , their high computational cost required, in particular for SampEn, may render its use unsuited for a hypothetical real-time application aimed at detecting hypoglycemic events from EEG. The aim of the present chapter is to assess if nonlinear indexes originally developed for the representation of chaotic systems, such as the fractal dimension, and already used in the literature to investigate EEG signal complexity [93] [94] [95], and two new indices reflecting both signal amplitude and frequency properties [96] are as sensitive as SampEn to HYPO and may thus lead to the same conclusions, in terms of signal characteristics, with lower computational cost, i.e. linear versus quadratic. In particular, we investigate how EEG *complexity* can be assessed through features extraction based on Higuchi's fractal dimension [97], and we compare its computational cost with SampEn. However, as demonstrated in several works, e.g. [98], EEG signal complexity can be assessed using various methods, with different degree of computational burden. The methods proposed in this chapter could be of practical relevance, because a reduced computational cost can allow the simultaneous computation of more features and/or the grouping of multiple assessments temporally consecutive.

## 4.2 Methods

### 4.2.1 Sample Entropy

Before focusing on fractal dimension measure, a brief overview on SampEn is presented. To calculate SampEn for an evenly sampled time-series $\{s(k)\}, k = 1, 2, ..., N$ , a positive integer $m$ (pattern length) is first chosen. Then, $(N \breve{} m)$ $m$-dimensional vectors $x_m(i)$ with $i = 1, 2, ..., N - m$, are defined as

$$x_m(i) = [s(i)...s(i + m - 1)]^T \tag{4.1}$$

where $i$-th vector $x_m(i)$ is made up of $m$ consecutive elements picked up from the original time-series, starting from the $i$-th element. Given a positive real tolerance parameter $r$, the quantity $C_i^m(r)$, for each $i = 1, 2, ..., N - m$, is defined as

$$B_i^m(r) = \frac{\#\ of\ \ vectors\ \ x_m(j), j \neq i : d[x_m(i), x_m(j)] \leq r}{N - m - 1} \tag{4.2}$$

where, in the numerator, $j$ ranges from 1 to $N - m$ and the quantity $d[x_m(i), x_m(j)]$, representing the distance between two vectors, is defined for $k = 1, ..., m$ as

$$d[x_m(i), x_m(j)] = max(|s(i + k - 1) - s(j + k - 1)|) \tag{4.3}$$

and is equal to the absolute value of the difference between corresponding elements of the two considered vectors having, among the others, the greatest value. For each $i = 1, 2, ..., N-m$, the ratio that appears in Eq. 4.2 is obtained dividing the number of vectors $x_m(j)$ having a distance from $x_m(i)$ lower than the tolerance $r$ by the overall number of comparisons (that is equal to $N - m - 1$, because $j = 1, 2, ..., N - m$ and the comparisons are performed

for $i \neq j$. The mean value over $i$ of the logarithms of $B_i^m(r)$ is then calculated:

$$B^m(r) = \frac{1}{N-m} \sum_{i=1}^{N-m} B_i^m(r) \tag{4.4}$$

and the quantity $B^m(r)$ is defined. Increasing the vector length from $m$ to $m+1$, the quantity $A^m(r)$ is obtained as well, and, eventually, SampEn is calculated as

$$SampEn(s, m, r) = -ln \frac{A^m(r)}{B^m(r)} \tag{4.5}$$

The computational complexity of the SampEn algorithm is O($N^2$) because two loops are required, one for $B^m(r)$ and one for $B^{m+1}(r)$.

As a development of SampEn, the MSE approach may be considered to investigate the complexity of a time-series, assessing how its entropy varies at increasing temporal scales [83] [82] [99] [100] [101] [102] . In brief, from the original time-series $\{s(1), s(2), ..., s(N)\}$, a new time-series $\{y(j)^\tau\}$ is defined as

$$y_\tau(j) = \frac{1}{\tau} \sum_{i=(j-1)\tau+1}^{j\tau} s(i), \;\; 1 \leq j \leq \frac{N}{\tau} \tag{4.6}$$

where the integer positive parameter $\tau$ represents the chosen time scale. Then, SampEn is computed for several values of $\tau$.

$$MSE(s, \tau, m, r) = SampEn(y_\tau, m, r) \tag{4.7}$$

In practice, the MSE approach reduces the length of the original time-series by averaging $\tau$ consecutive samples belonging to non-overlapping blocks. This coarse-graining procedure allows obtaining averaged down-sampled versions of the original time-series, whose SampEn values are related to the complex fluctuations of the original signal running at temporal scales $\tau$ times larger than the sampling time used to acquire the data. At a scale

factor of $\tau$, the execution time required to calculate the SampEn of the coarse-grained time series is $O((N/\tau)^2)$. Therefore, the overall computational complexity of the MSE approach, at $n$ increasing temporal scales is $O(\sum_{\tau=1}^{n}(N/\tau)^2)$. In Fig. 4.1, an example of the application of MSE in T1D subjects is reported. SampEn value increases at small time scales ($\tau$ from 1 to 5) and monotonically decreases as the time scale becomes larger ($\tau$ from 5 to 40), with a slope steeper at medium temporal scales ($\tau$ from 5 to 20) than at the largest ones ($\tau$ from 20 to 40). The initial increase in the entropy values could be related to the fact that the MSE procedure initially produces an effective decorrelation of a signal with a finite correlation time [103]. However, as the analyzed temporal scale increases, the number of averaged samples increases as well, and erratic fluctuations of the signal are attenuated, inducing a progressive entropy decrease, suggesting that the long-range temporal correlations of the EEG, which are strictly related to its complexity, are degraded at low BG levels and damaged in HYPO [48].

### 4.2.2 Features extraction based on fractal dimension concept

The fractal dimension provides a complexity index that describes how the measure of the length of a curve $L(k)$ changes depending on the scale $k$ used as unit of measurement. Different approximation techniques can be used to estimate fractal dimension [104]. Among these different approaches, Higuchi's algorithm [97] is often employed in EEG analysis to estimate the fractal dimension $D$ [94] [95] [105]. The Higuchi's standard approach calculates fractal dimension of time series in the time domain, and is based on the $log(L(k))$ vs $log(k)$ curve computed as follow:

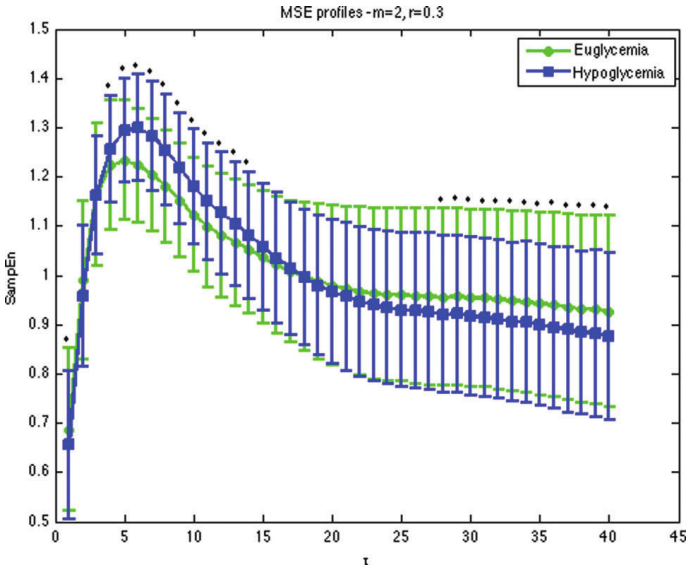


FIGURE 4.1: Multiscale entropy (MSE) profiles obtained within EEG in T1D patients in EU (green line with solid circles) and HYPO (blue line with solid squares) with $m = 2$ and $r = 0.3$. Data are mean $\pm$ sd values. Stars on the top of the bars indicate statistically significant differences ($p < 0.05$) between sample entropy (SampEn) values at the considered temporal scale. Reproduced from [48]

- For each sample $i$ of the EEG epoch $S$, absolute differences between the values $S(i)$ and $S(i-k)$ (i.e. samples at distance $k$) are computed, considering $k = 1, ..., k_{max}$;

- Each absolute difference is multiplied by a normalization coefficient that takes into account the different number of samples available for each value of $k$. The computation of this coefficient is based on the starting point $m = 1, ..., k$ and on the total number ($N$) of samples of an epoch;

- $L(k)$ is computed by summing the obtained values and dividing by $k$;

$$L(k) = \frac{1}{k}\sum_{m=1}^{k}\left[\frac{1}{k}(\sum_{i=1}^{q}|S(m+ik) - S(m+(i-1)k)|)\frac{N-1}{qk}\right] \tag{4.8}$$

  where $q = int[(N-m)/k]$;

- The $log[L(k)]$ vs $log(k)$ curve, referred in the following as $l_k$, is finally derived.

By definition, if $L(k)$ is proportional to $k^{-D}$ (i.e. $log(k)$ and $log[L(k)]$ have a linear relationship) for $k = 1, 2, ..., k_{lin}$, then the curve is fractal with dimension $D$. Consequently, $k_{lin}$ is the maximum $k$ for which $L(k)$ is proportional to $k^{-D}$ and $D$ is estimated by ordinary least squares as the linear coefficient of the regression line of the $l_k$ curve for $k = 1, 2, ..., k_{lin}$. Therefore, the Higuchi's fractal dimension increases as the signal irregularity increases.

The non-linear part of the $l_k$ curve ($k > k_{lin}$) presents an oscillatory behavior whose characteristics depend on the periodicity of the signal itself [96]. In Fig. 4.2, the effect of signal periodicity on Higuchi's curve is represented for a cosine wave with frequencies 2.5 Hz (panel a), 5 Hz (panel b) and 7.5 Hz (panel c) and adding pseudo-normal random noise ($sd = 0.2$) to the cosine wave with frequency 2.5 Hz (panel d). In panels e-h, it can be seen that the first part of the curve is approximately linear, while the remaining part presents oscillations (i.e. negative spikes with respect to the linear fit) that depend on the frequency of the original signal, with higher frequency resulting in a larger number of negative spikes. The presence of additive noise (panel h) slightly affect the curve, indeed the presence and latency of its negative oscillations is preserved.

In addition to Higuchi's fractal dimension, we also extract two additional features [96], which consider a wider domain of

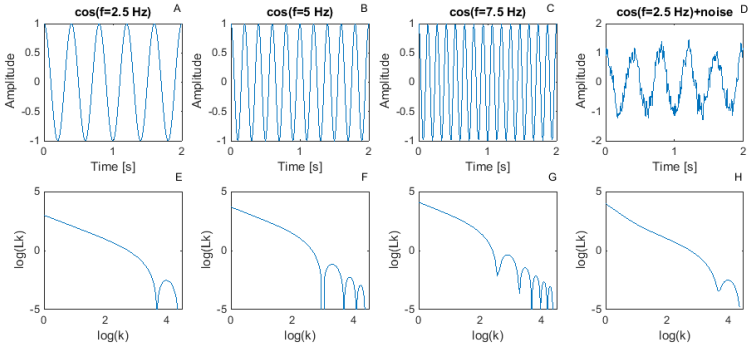


FIGURE 4.2: Examples showing the effect of signal periodicity on Higuchi's curve. The upper panels show the original signals, generated as cosine waves with frequencies 2.5 Hz (A and D), 5 Hz (B) and 7.5 Hz (C). The lower panels (E-H) show the corresponding Higuchi's curve. The last signal (D) is generated adding pseudo-normal random noise, with standard deviation equal to 0.2, to the cosine wave with frequency 2.5 Hz.

the $l_k$ curve with respect to the Higuchi fractal dimension. The first additional feature evaluates the deviation (i.e. the sum of squares of the residuals) of the $l_k$ curve from the regression line computed on its linear region. The second additional feature is a tortuosity measures $\tau$ of $l_k$. It consists in a measure of the rate at which the curve is changing with respect to its coordinates changes ($x = log(k)$ and $y = log(L(k))$), by using their first and second partial differences:

$$\tau_{l_k} = \sum_{n=3}^{k_{max}} \left| \frac{\Delta x(n)\Delta^2 y(n) - \Delta^2 x(n)\Delta y(n)}{[(\Delta x(n))^2 + (\Delta y(n))^2]^{3/2}} \right| \tag{4.9}$$

where $\Delta x(n) = x(n) - x(n-1)$, $\Delta^2 x(n) = \Delta x(n) - \Delta x(n-1)$, $\Delta y(n) = y(n) - y(n-1)$, $\Delta^2 y(n) = \Delta y(n) - \Delta y(n-1)$. A complete description of this tortuosity measures can be found in [106]. These two features increase as the signal regularity and

periodicity increase.
The linear region is here defined considering $k_{lin} = 6$, according to [94], while the two other features are computed considering also the non-linear region up to $k_{max} = 30$ according to [96].

## 4.3 Implementation

The analysis is applied to P3-C3 EEG derivation in order to compare our fractal dimension indicators to SampEn results obtained in [48] and it is also evaluated on the same database of [48].

### 4.3.1 Preprocessing

For each subject, from the two 1-h intervals corresponding to EU and HYPO conditions, the P3-C3 EEG derivation was chosen since the EEG signal from this scalp position is highly affected by hypoglycemic events [30] [35]. The P3-C3 EEG derivation in EU and HYPO was split into epochs of 4 seconds length, with 2 seconds overlap. Epoch length and overlap were chosen as a trade-off between the amount of available data samples required to calculate the features for each epoch and the readiness required for prompt identification of a physiological change.

EEG data can be affected by several sources of noise, such as body movements and propagation of bioelectrical muscles potentials, which are likely to sum up into the electroencephalographic signal generated by the brain. Consequently, recorded EEG signals may show trends, low frequency oscillations and baseline changes due to these components. In order to remove these artefacts a detrending step to each EEG epoch was applied to correct drifts and linear trends. Briefly, a first order model consisting of an offset plus a linear trend was fitted to each epoch, estimated and then subtracted from the epoch itself. Furthermore,

for each epoch, if the value of one or more of its samples was greater than 100 $\mu V$ or lower than -100 $\mu V$, the epoch was considered as affected by artefacts and thus not considered for the analysis (on average, 0.4% epochs rejected per subject).

## 4.4 Results

For each 4-s EEG epoch in EU and HYPO, the fractal dimension features described in the previous section were computed. Moreover, the results obtained by the fractal analysis were compared with the SampEn results ($m = 2, r = 0.3$) obtained in [48] on the same dataset, where the 1-h EEG intervals in eu- and hypoglycemia were divided in 60 epochs lasting 60 seconds (12000 samples) to guarantee that the shortest analyzed time-series ($\tau = 40$) consisted of at least 300 samples. Indeed, SampEn was derived by coarse-grained time series, obtained by calculating the arithmetic mean of $\tau$ neighboring values without overlapping, thus reducing the original time- series by a scale factor $\tau$. In [48], the difference between EEG SampEn in EU and HYPO was relevant with no scale factor and at the largest temporal scales ($\tau = 25 : 40$). Thus, we chose $\tau = 1$ (i.e. no scale factor, the original time series was not decimated) and $\tau = 35$ (i.e. the scale factor that allowed the most relevant difference between the two glycemic states) for the comparison of SampEn with our results. We refer the reader to [48] for further parameter details in SampEn computation.

The proposed features based on fractal dimension show different distributions in the two glycemic states, denoting a decrease in the EEG signal complexity in all the subjects during HYPO. Indeed, as visible in Fig. 4.3 for a representative subject where the distributions of the features in EU (green distribution) and HYPO (blue distribution) are reported, the Higuchi's fractal

dimension tends to decrease shifting from EU to HYPO, while the fractal dimension residuals and tortuosity tend to increase. These results are confirmed across all subjects, Fig. 4.4.

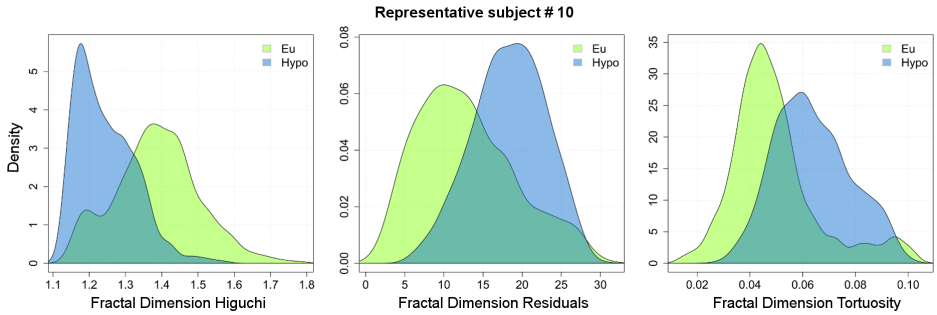


FIGURE 4.3: Distributions of the values for 4-s epochs in EU (green distribution) and HYPO (blue distribution) of Higuchi's fractal dimension (left), the residuals (middle) and tortuosity (right) for the representative subject id 13.

The indices obtained from both the eu- and the hypoglycemic state were compared by a two-sided Wilcoxon rank sum test to identify significant changes in the signal properties in two 1-h intervals corresponding to EU and HYPO. A statistically significant decrease of the standard Higuchi fractal dimension was found from eu- to hypoglycemic state in 18 over 19 subjects ($p$ always < 2e-22, except for subject with id 27, for which $p = 0.248$). A statistically significant increase for all subjects was found for residuals and tortuosity features ($p < 4e - 6$ and $p < 0.005$, respectively). The decrease of Higuchi fractal dimension and the increase of the two additional features in HYPO highlight a reduction of the EEG signal complexity in this physiological condition. Moreover, this reduction of signal irregularity agrees with the progressive entropy decrease highlighted by the monotonically decrease in SampEn values in EEG signal affected by HYPO, found in [48]. Thus, all analyzed methods agree in associating a reduction of

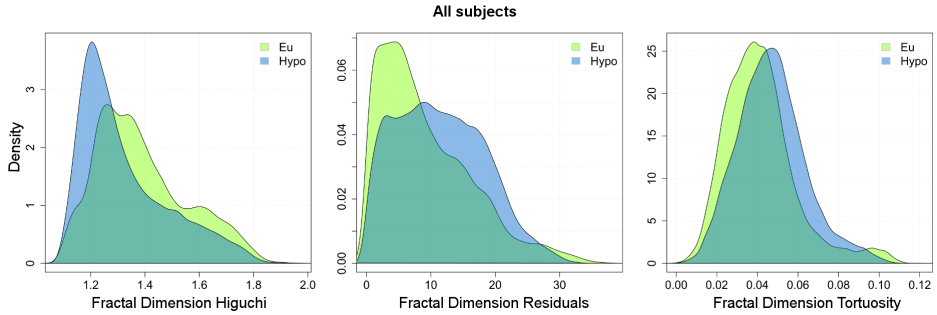


FIGURE 4.4: Distributions of the values for 4-s epochs in EU (green distribution) and HYPO (blue distribution) of Higuchi's fractal dimension (left), the residuals (middle) and tortuosity (right) for all subjects.

the irregularity of EEG signal to the hypoglycemic state, which is in agreement with the progressive loss of cognitive function and altered cerebral activity.

Receiver operating characteristic (ROC) analysis was performed to quantitatively measure the capability of each feature to identify changes in the signal properties related to the different glycemic state. For each subject, the ROC curve was computed by plotting the true positive rate (sensitivity) versus the false positive rate (1-specificity), and the area under the curve (AUC) was measured. The AUC is a measure of how well a parameter can distinguish between two groups: it can vary from 0 to 1 and if equal to 1 indicates maximal sensitivity and specificity, and thus perfect discrimination between the two glycemic states. AUCs were calculated for Higuchi fractal dimension, residuals and tortuosity features. In Fig. 4.5, the results of ROC analysis for all subjects are depicted. The AUC scores obtained by the features based on fractal dimension on the majority of the subjects denote their effectiveness in extracting useful information with discriminatory power from the EEG signal. A two-sided Wilcoxon rank sum

test was applied to compare the AUCs obtained by the different features, and no statistically significant difference was found between features ($p > 0.18$).

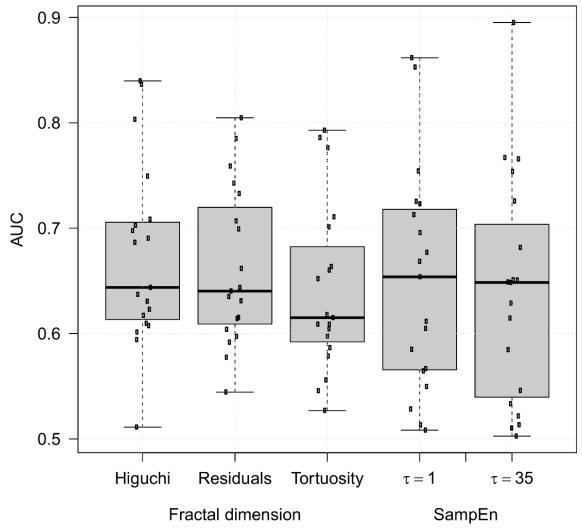


FIGURE 4.5: Results of the ROC analysis. Area Under the Curve (AUC) obtained by each feature for all subjects is reported. In each box, the central thick line is the median value, the edges of the box are the 75th and 25th percentiles, the whiskers extend to the most extreme data points that are not outliers. Each AUC is also plotted individually.

In order to quantitatively compare the results obtained by the fractal analysis with that obtained as in [48], AUCs were also derived from the SampEn values obtained in [48] from 60 epochs lasting 60 seconds with no scale factor ($\tau = 1$) and at a scale factor $\tau = 35$ (Fig. 4.5). Similar AUC values were obtained by the different methods, and no statistically significant difference ($p > 0.36$) was found between the AUCs obtained from 4-s

epochs by each fractal feature versus the AUCs obtained from 60-s epochs by SampEn. A comparison between the fractal features and SampEn on epochs of the same length was not performed because 4-s epochs ($N = 800$) do not contain enough samples to accurately compute SampEn at different scale factors, and on 60-s epochs ($N = 12000$) the computational cost of fractal features and of SampEn with no scale factor would be too high for a real-time application.

The computational cost of EEG complexity estimation assessed by fractal analysis from 4-s epochs ($N = 800$ samples) is $O(KN)$. Indeed, the computation of $L(k)$, see Eq. 4.8, requires the execution of $N$ mathematical operations for each $k = 1 : K$, with $K$ smaller than $N$ (in this work, $K = k_{lin} = 6$ for Higuchi's fractal dimension, $K = k_{max} = 30$ for residuals and tortuosity, and $K = k_{max} = 30$ for all of them simultaneously). The short epochs length and the low computational cost allow fractal features to provide frequent assessment of the physiological state, which is essential for a useful real-time detection of HYPO.

On epochs of the same length (4 seconds), entropy based methods, i.e. SampEn, could be applied without a scale factor, but their computational cost, $O(N^2)$, would be extremely higher than the one of fractal analysis. This computational cost can be drastically reduced using SampEn at a scale factor $\tau$, $O((N/\tau)^2)$. However, this requires a greater number of samples [107], that involves longer epochs, i.e. 60-s epochs ($N = 12000$). The high number of samples to be simultaneously analyzed makes it difficult to be implemented in a real-time application and the long time interval of each epoch can potentially affect the readiness to identify the hypoglycemic state.

## 4.5 Discussion

The present chapter investigated if algorithms based on Higuchi's fractal dimension can reveal changes in the complexity of the EEG signal induced by HYPO. Using the P3-C3 EEG derivation data, we showed that the proposed features based on fractal dimension could be used to assess changes in EEG complexity, which occur during HYPO, likely related to progressive loss of cognitive function and altered cerebral activity. The information content of these indices leads to results in line with that achieved by nonlinear entropy-based indicators like SampEn. Indeed, the decrease of the Higuchi fractal dimension and the increase of the residuals and the tortuosity features highlight the same decrease of the EEG signal complexity in HYPO condition.

# Chapter 5

# Microstate analysis

## 5.1 State of the art

It is interesting, for a better understanding of brain functioning in hypoglycemia, to investigate further approaches which consider several EEG channels at the same time. In particular, the aim of this chapter is to better understand the changes in brain network dynamics that lead to the theta and alpha power increase during hypoglycemia by performing topographical EEG analysis. By displaying the resting EEG electric potential amplitude of all channels as a topographic voltage map at each time point, it is possible to define the series of quasi-stable topographic configurations, which last several tens of milliseconds [108] [109] [110] [111]. In particular, Lehmann was the first to observe that the topography of the map representing resting EEG electric potential amplitude does not randomly and continuously change, but remains stable for a length of time and then abruptly changes into a new configuration and so on [108]. Moreover, he proposed that these stable maps were the basic blocks of the information processing and baptized the term *functional microstates* for these *athoms of thoughts*. The topographies of the microstates are similar among different studies: 4-8 classes of topographies are usually identified to explain most of the data [112]. For instance, in [113], authors presented normative microstates data for resting

EEG obtained from a database of 496 subjects between the age of 6 and 80 years. Fig. 5.1 shows the topographies of the four microstates classes which were found in the study arranged in the following order: microstate class A with a left occipital to right frontal orientation, class B from right occipital to left frontal, class C with a symmetric occipital to prefrontal orientation and class D symmetric, but with a frontocentral to occipital axis. Map areas of opposite polarity are arbitrarily coded in red and blue using a linear color scale, left ear is left, nose is up. The four topographies extend over wide scalp areas and are likely to represent global brain electric events. From these microstates classes, several parameters can be extracted, e.g., the mean duration, i.e., how each microstates class lasts before abruptly changing in the following map. In Fig. 5.2, the duration across age of the microstates classes of Fig. 5.1 are reported: the mean duration was circa 80-100 ms and microstates class C dominated during adolescence. Thus, EEG seemed to be able to measure these resting states as well as the other imaging procedures such as functional imaging [114], but also with an higher temporal resolution (ms) [112] with the final aim to understand how the brain works.

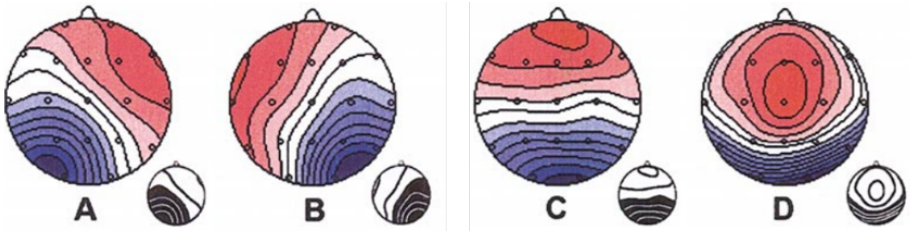


FIGURE 5.1: Normalized mean equipotential contour maps of the four microstates classes (A–D) from study [113]. Reproduced from [113]

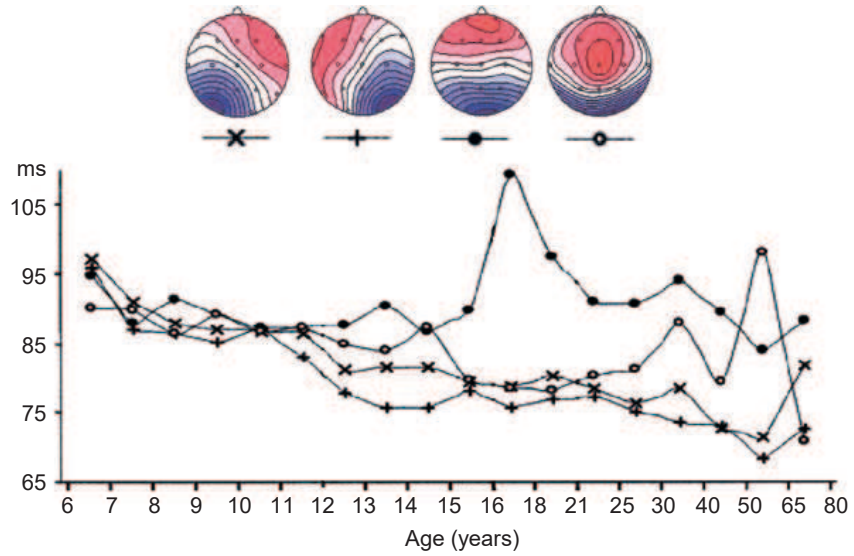


FIGURE 5.2: The duration across age for each map of the four dominant microstates of the study [113] is shown. The mean duration is circa 80-100 ms. Microstate class C dominates during adolescence. Reproduced from [112]

Indeed, these different topographical configurations of electric potentials over the multichannel electrode array, i.e., the different microstates, are thought to be related to different functional resting state networks as known from fMRI. Many studies have discovered significant changes in the resting-state microstates series in a variety of neuropsychiatric disorders [115] [116] [117] and behavioral states [118] [119]. To understand how EEG microstates correlate with parameters extracted using analytical methods, e.g., relative power in the canonical frequency bands, is still an open question. Since several works have proven that a power increase in the low frequency EEG bands takes place during HYPO with respect to EU (Chapter 3) and differences in terms of signal complexity have been also evidenced (Chapter 4),

in this chapter we investigate if there are significant differences in the time-course of microstates in HYPO compared to EU in the broadband, delta, theta, alpha and beta frequency range.

## 5.2 Methods

### 5.2.1 Averaged topographies

The analysis is based on a two-stage process to obtain the prototype topographies, which best explain most of the signal variance, in EU and HYPO. The following analysis was performed in data filtered in broadband [1-40] Hz, in delta, theta, alpha, and beta frequency bands by a 4-order Butterworth filter. First, for each patient, the time points of the maximum Global Field Power (GFP), i.e.,

$$GFP_c(t) = \sqrt{\frac{\sum_{i=1}^{N}(c_i(t) - \overline{c}(t))^2}{N}} \tag{5.1}$$

where $c_i(t)$ is the voltage potential at the electrode $i$ and $\overline{c}(t)$ is the average voltage potential of all electrodes at time point $t$ and $N = 19$ is the number of electrodes, were selected as the moments of high global neuronal synchronization, from EU and HYPO (Fig. 5.3 panel (a)). For each patient, the topographies of these time points (Fig. 5.3 panel (b)) were then clustered independently using a k-means clustering approach (Fig. 5.3 panel (c)). The optimal number of clusters was selected based on the overall performance of multiple clustering validity criteria [110] [111] [120] [121] [122] [123] [124] [125].

In second step, the optimal clusters of each patient in EU and HYPO were again clustered together to find the most common templates maps across the two glycemic conditions. Finally, these most common templates were fitted back to the original EEG in EU and HYPO, and each time point $t$ was labeled with the

cluster maps based on Global Map Dissimilarity (GMD) measure

$$GMD(t) = \sqrt{\frac{1}{N}\sum_{i=1}^{N}\left(\frac{c_i(t)-\overline{c}(t)}{GFP_c(t)} - \frac{v_i(t)-\overline{v}(t)}{GFP_v(t)}\right)^2} \tag{5.2}$$

where $c_i(t)$ is the voltage potential at the electrode $i$ and $c(t)$ is the average voltage potential of all electrodes at time $t$ in the map $c$ while $v_i(t)$ is the voltage potential at the electrode $i$, $v(t)$ is the average voltage potential of all electrodes at time $t$ in the map $v$ and $N = 19$ is the number of electrodes. The GMD is equivalent to the spatial Pearson's product-moment correlation coefficient between the potentials of the template map and the instant topography. This resulted in the microstates sequence (Fig. 5.3 panel (d)). Microstates analysis was performed with the freely available CARTOOL software [126]. In Fig. 5.3, this steps are schematized: for each time point (a), the potential distribution map was calculated (b). Then a k-means cluster analysis was applied to all maps. A cross-validation criterion identified four dominant maps (c). Fitting these maps back to the original data revealed that each map appeared repeatedly and dominated during certain time segments, i.e., the microstates. These microstates are color-coded in the curve of Global Field Power at the bottom, and marked by letters under this curve; they were classified according to the standard microstates classes (d).

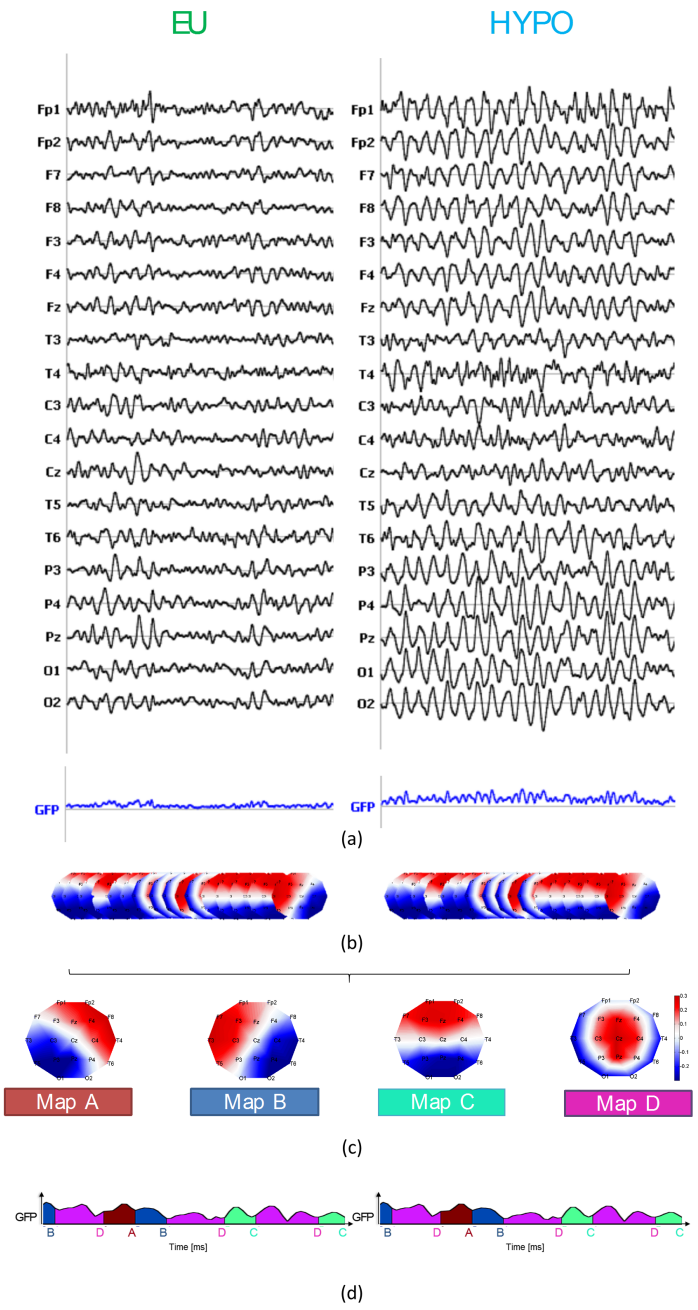


FIGURE 5.3: Qualitative example of microstates segmentation of EEG signal in both glycemic states using the cluster analysis.

### 5.2.2 Microstates parameters

To compare the microstates sequences between EU and HYPO, the following parameters were computed:

1. the total time coverage (TTC) giving the percent of total time in the EEG recording, covered by each microstate class,
2. the global explained variance (GEV) for each microstate class, calculated as the sum of the squared spatial correlation, weighted by the GFP at each time point, and giving a ratio of how well the template topography describe the whole data set [126] and,
3. the Occurrences/s describing the average number of appearances for the same microstate per second.

Finally, a MANOVA was performed on the results of microstates parameters for each frequency band, after checking all MANOVA hypotheses (normally distribution of all dependent variables by a Lilliefors test, linear relationships between them by scatter plots, and homogeneity of variance and covariances by Box's M test). In particular, the Pillai's trace criterion was exploited because it is considered the most powerful and robust, also if the homogeneity of covariances is not verified. If the MANOVA revealed a significant multivariate main effect, Student's t tests with p-value corrected by false discovery rate (Benjamini–Yekutieli procedure [13]) were applied between the microstates parameters results in EU and HYPO.

## 5.3 Results

The averaged topographies obtained following the procedure described in the previous sections are reported in Fig. 5.4. In particular, the analysis for both glycemic conditions in all subjects

results in four topographies from all the frequency bands. These four topographies were named map A, B, C and D, according to the microstates literature convention. In Fig. 5.4, only the topography's relative configuration, but not its polarity is considered. These four template topographies are displayed per definition with red color towards the front. The light-blue squares highlight maps with significant difference of microstates parameters between EU and HYPO: specifically, map D displays significant difference in its microstates parameters in all frequency bands. Moreover, after looking at all the maps topographies in Fig. 5.4, we can note that map D remains stable in all the frequency bands, i.e., there are not differences in the configuration of this map across the frequency bands.

In Table 5.1, multivariate tests results of MANOVA applied to microstates parameters results, i.e., TTC, GEV and Occurrences/s (compound effect) in EU and HYPO (group effect) for all T1D patients are reported. After testing that there was a significant difference in the results of microstates parameters in HYPO compared to EU, results of microstates parameters for both glycemic conditions in all subjects from data filtered in all bands are computed and depicted in Fig. 5.5. In particular, during HYPO, there were:

- an increase of Occurrences/s of map C ($p = 0.0071$) and a decrease of TTC, GEV and Occurrences/s of map D ($p < 0.01$) in the broadband;
- an increase of TTC, GEV and Occurrences/s of map B ($p < 0.0081$) and a decrease of TTC, GEV and Occurrences/s of map D ($p < 0.02$) in delta band;
- an increase of TTC of map B ($p = 0.0081$) and a decrease of TTC, GEV and Occurrences/s of map D ($p < 0.0066$) in

TABLE 5.1: MANOVA (Pillai's trace)

| | | f | p | Trace |
|---|---|---|---|---|
| Broadband | Group | 6.8672 | 2.1354e-04 | 0.8290 |
| $[1-40]$ Hz | Compound | 1.4807e+03 | 0 | 0.9989 |
| | Interaction | 2.5305 | 0.0389 | 0.6073 |
| Delta band | Group | 11.9611 | 5.0534e-06 | 0.8941 |
| $[1-3.4]$ Hz | Compound | 663.6563 | 0 | 0.9975 |
| | Interaction | 13.5025 | 1.5464e-06 | 0.8919 |
| Theta band | Group | 2.4489 | 0.0448 | 0.6335 |
| $[4-8.7]$ Hz | Compound | 483.7364 | 0 | 0.9966 |
| | Interaction | 2.6232 | 0.0336 | 0.6158 |
| Alpha band | Group | 17.0827 | 3.7047e-07 | 0.9234 |
| $[9-12]$ Hz | Compound | 858.7760 | 0 | 0.9981 |
| | Interaction | 6.0999 | 4.0019e-04 | 0.7885 |
| Beta band | Group | 7.2614 | 1.4977e-04 | 0.8368 |
| $[14-17]$ Hz | Compound | 1.2135e+03 | 0 | 0.9987 |
| | Interaction | 4.5466 | 0.0023 | 0.7353 |

theta band; a decrease of TTC and Occurrences/s of map D ($p < 0.0081$) in beta band

- finally, an increase of Occurrences/s of map C ($p = 0.0047$) and a decrease of TTC and Occurrences/s of map D ($p < 0.0081$) in beta band

(the false discovery rate was controlled by Benjamini-Hochberg procedure [127]).

To sum up, we can state that there is an evident and significant decrease of TTC and Occurence/s per second of map D during HYPO respect to EU in all frequency bands.

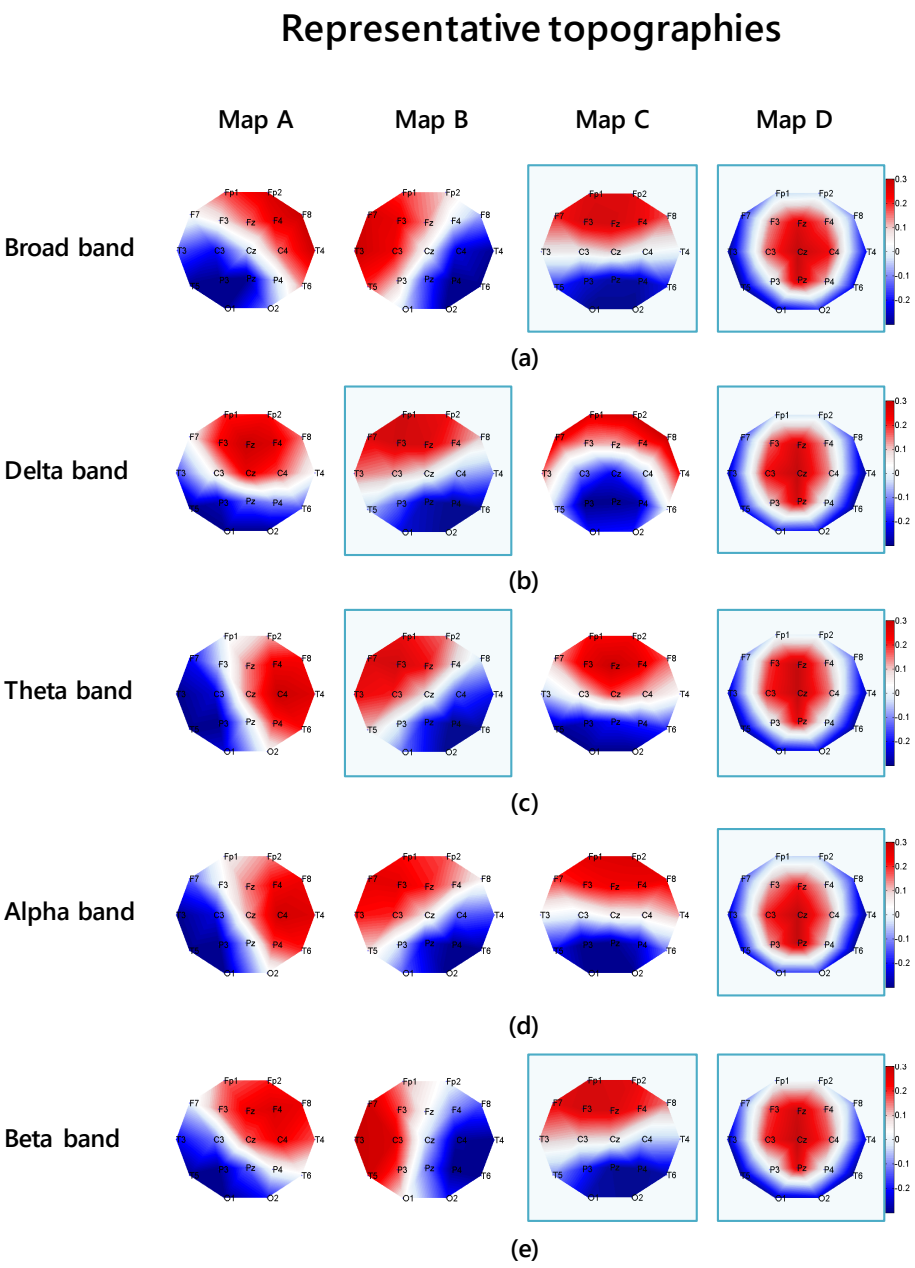


FIGURE 5.4: 4 most representative topographies for both glycemic conditions in all subjects from broadband data [1-40] Hz, delta band [1-3.4] Hz, theta band [4.8-7] Hz, alpha band [9-12] Hz, beta band [14-17] Hz, named map A, B, C and D, according to the microstates literature convention. Map D displays significant difference in its microstates parameters in all frequency bands.

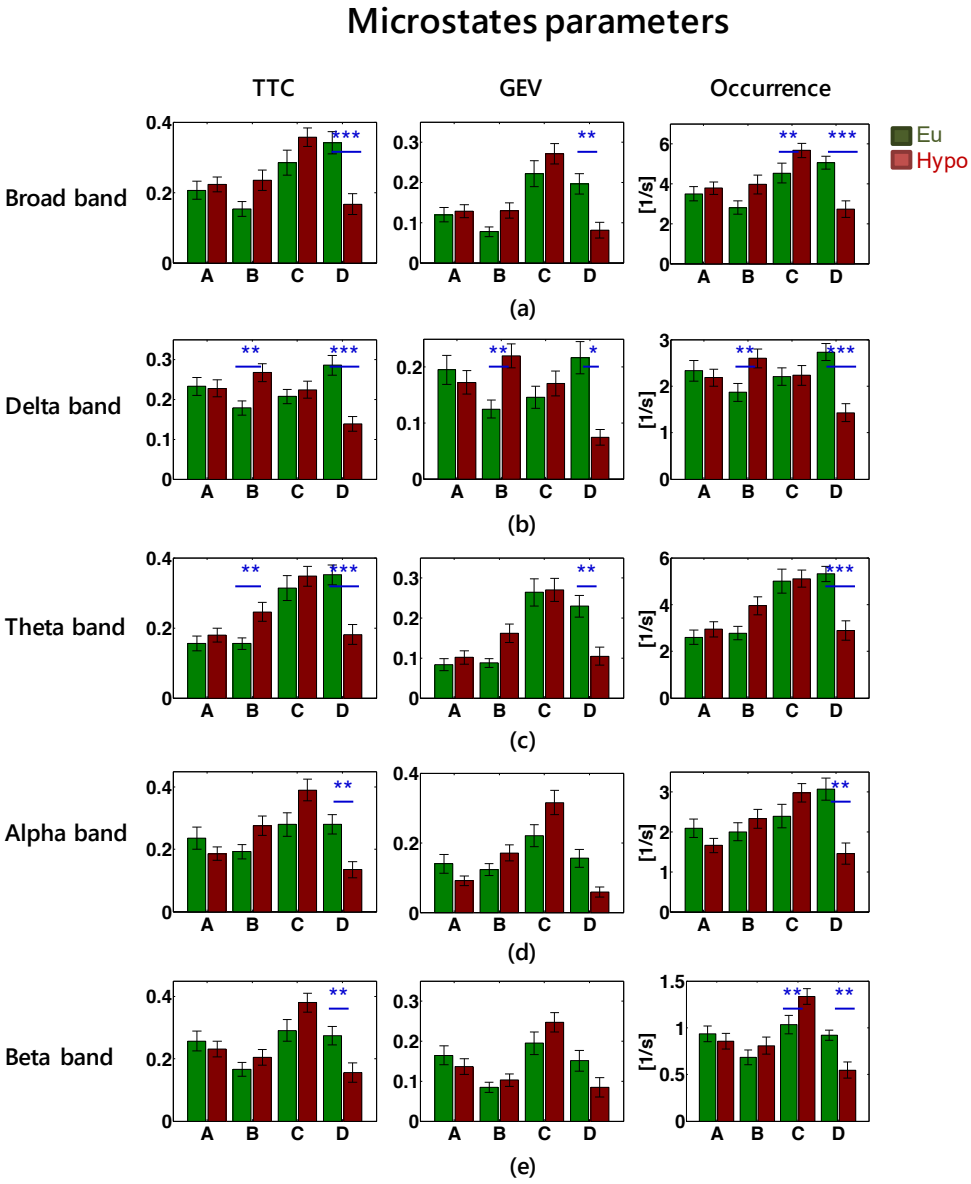


FIGURE 5.5: Results of microstates parameters for both glycemic conditions in all subjects from data filtered in: broadband [1-40] Hz, delta [1-3.4] Hz, theta [4.8-7] Hz, alpha [9-12] Hz and beta [14-17] Hz EEG frequency bands. Significant differences between EU and HYPO results are reported by one star for $p_{value} \leq 0.05$, two stars for $p_{value} \leq 0.01$ and three stars for $p_{value} \leq 0.001$.

## 5.4 Discussion

In this chapter, we investigated if there were significant differences in the time-course of microstates in HYPO compared to EU in the broadband, delta, theta, alpha and beta frequency range. We found an evident and significant decrease of TTC and Occurrences/s of map D during HYPO respect to EU in all frequency bands. This result might support the hypothesis that the changes in the frequency domain (Chapter 3) and the decrease of the EEG signal complexity in HYPO (Chapter 4) have in common the same resting EEG electric potential amplitude map.

# Chapter 6

# Behavioral performance and correlation among EEG quantitative features

## 6.1 State of the art

Recent studies have investigated the relationship between resting-state slow wave power, healthy aging and cognitive performance [128]. In particular in [128], authors found that healthy aging was accompanied by a marked and linear decrease of resting-state activity in the slow frequency range, i.e., $[0.5 - 6.5]$ Hz. Moreover, the effects of slow wave power on cognitive performance were expressed as interactions with age: for older subjects ($> 54$ years) the change in delta and theta power in temporal and central regions was positively associated with perceptual speed and executive functioning, underlining the important role of slow wave oscillations in neurocognitive function. The works [129] [130] [131] [132] supported the hypothesis that neural oscillations coordinate information transfer in the brain, support plasticity processes and subserve important perceptual and cognitive functions such as sensory feature binding, speech perception, memory and attention.

In this chapter, we want to investigate the cognitive performance during HYPO for T1D patients and the relationship with the increase in power in low frequency bands and the change in the microstates parameters. The cognitive performance was not compared to the results of functional connectivity (Chapter 3) and complexity analysis (Chapter 4) because these two analyses were limited to a subset of EEG channels.

## 6.2 Results

### 6.2.1 Behavioral performance

All subjects performed the Stroop test and the TMT B during the three glycemic periods, i.e., EU, HYPO and the recovery after the period in HYPO. In Fig. 6.1, the results of the cognitive tests for all subjects are reported. Firstly, we can note that during the recovery (light green in Fig. 6.1), the results for each of the tests are comparable with the results during the period of EU before entering in HYPO (dark green in Fig. 6.1). Thus, we can state that the visible patients drop in performance during HYPO was not due to tiredness (the HYPO interval is about 4 hours after the start of the experiment in the hospital). Secondly, after applying paired Student's t-tests under the hypothesis of normal distribution of samples (Lilliefors test) otherwise, Wilcoxon rank-sign tests, a significant worsening during HYPO compared to EU was found in the performance of all the tasks ($p < 0.001$). In particular during TMT B, performances deteriorated up to 30% and during the Stroop test up to 15%, revealing the drop in visual attention, processing speed and selective attention during HYPO. We also replicated the analyses by dividing the subjects with and without awareness of HYPO, but no significant difference in the performance for the two groups were found. In Fig. 6.2, we reported

the results for each of the test for both groups in EU, HYPO and Recovery.

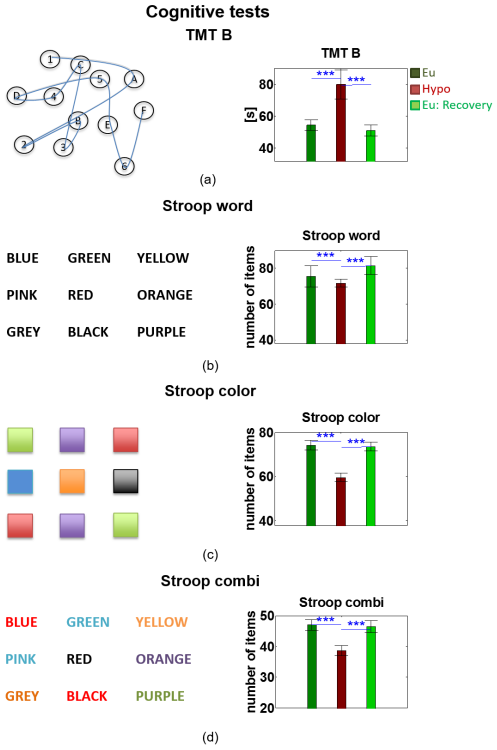


FIGURE 6.1: In panel (a), on the left, example of TMT B and, on the right, results of TMT B performance in EU, HYPO and Recovery by T1D patients. In panels (b, c, d), on the left, example of Stroop Color and Word Test; on the right, number of items named correctly by T1D patients in 45 s in EU, HYPO and Recovery. During HYPO, there is a significant worsening in the performance of all the tasks ($p<0.001$) while EU and Recovery conditions are comparable.

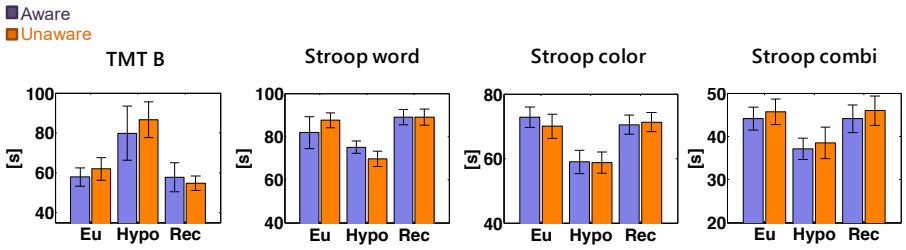


FIGURE 6.2: From left to right, results of TMT B and Stroop test in aware (violet) and unaware (orange) patients in EU, HYPO and Recovery. In all conditions, the performance for awareness patients is comparable with the one of unawareness subjects. There are not significant differences.

### 6.2.2 Correlation between cognitive tests and EEG quantitative measures

The goal of this section is to evaluate if there are any correlations among the cognitive impairment due to HYPO presented in the previous section, the altered topography and temporal dynamics of the brain electric microstates described in Chapter 5, and the altered power spectra presented in Chapter 3. In particular, we computed the sample linear partial correlation coefficients $r$ and their corresponding p-values between:

- the difference ($\Delta$) in EU and HYPO of the microstate parameters that results significantly different between the two different glycemic conditions;
- the difference in EU and HYPO of the absolute power in the theta, alpha and beta frequency bands in all electrodes;
- the difference in EU and HYPO of the results of neurocognitive tests;

while controlling for the effect of age and diabetes duration.

Before computing the correlation among the significant results obtained in the previous chapters, we controlled if there were differences in the results between hypo-aware and unaware patients in the most significant spectral power and microstate parameters results. As depicted in Fig. 6.3, there was only a light difference in the overall results between the two groups for microstates parameters. The difference between EU and HYPO is more significant in hypo-aware patients ($p < 0.01$) than in hypo-unaware ones ($p < 0.05$). Because of this slight difference in microstates, we compared all the results in all microstates maps.

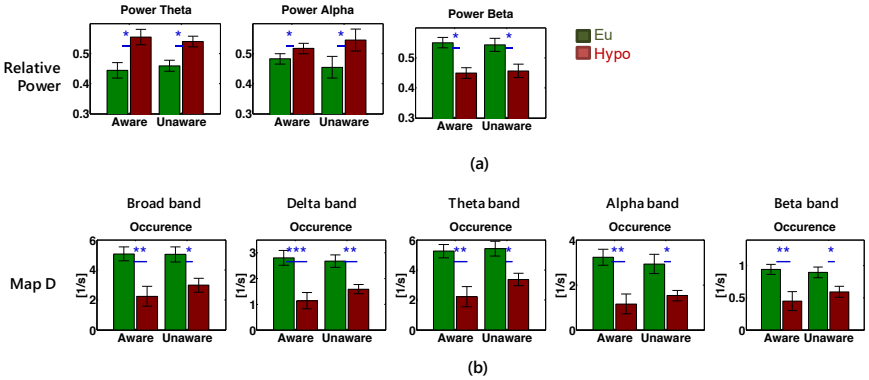


FIGURE 6.3: In panel (a), average power across all electrodes in theta, alpha (considering only T5- T6- P3- P4- Pz- O1- O2-A1A2) and beta frequency bands in EU, HYPO in the patients with hypo-awareness versus the patients with hypo-unawareness. There is not difference in the overall results between the two groups. In panel (b), results of microstate parameter Occurrences/s for map D. The difference between EU and HYPO is more significant in hypo-aware patients ($p < 0.01$) than in hypo-unaware ones ($p < 0.05$).

Although only qualitatively, we found a difference in map C between aware and unaware patients as depicted in Fig. 6.4.

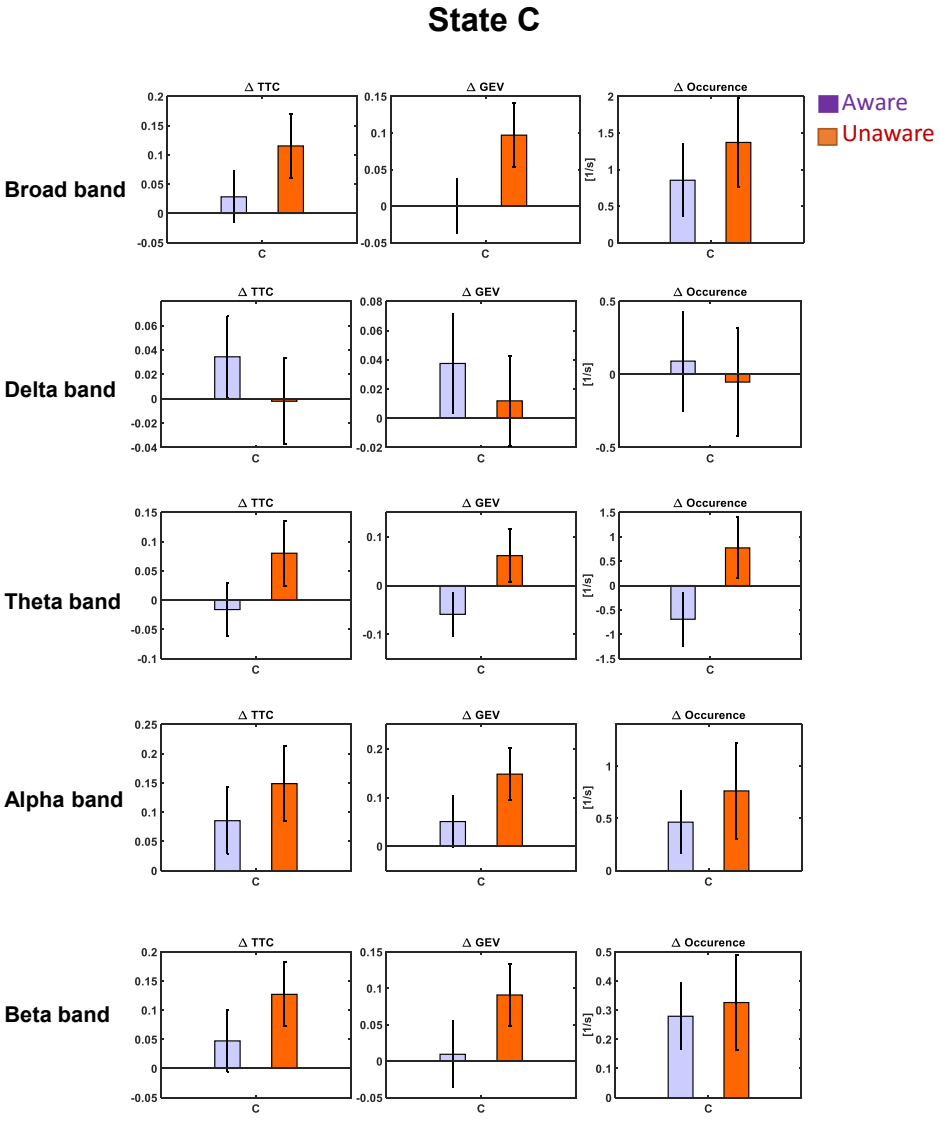


FIGURE 6.4: Microstates parameters of map C in all EEG frequency bands. Generally, Map C seems to be more present in unaware patients compared to aware patients during HYPO.

This result suggests that map C in unaware patients is generally more present during HYPO in accordance with [133], where authors showed that map C becomes more dominant when somatic awareness is reduced.

In Fig. 6.5 and 6.6, we reported the results between the variables that resulted significantly correlated. Fig. 6.5 reported the results of the magnitude of Pearson's linear correlation coefficients $|r|$ (colorbar) between the difference in the performance between EU and HYPO of TMT B and:

(a) the increase in power of theta band;

(b) the increase in power of alpha band;

(c) the decrease in power of the beta band during HYPO in all electrodes.

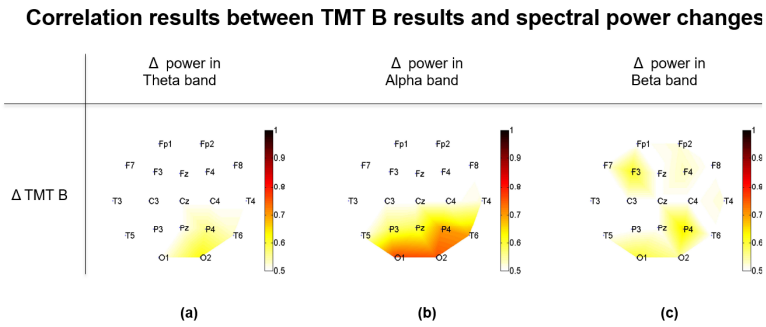


FIGURE 6.5: Results of the magnitude of Pearson's linear correlation coefficients $|r|$ (colorbar) between the difference in the performance between EU and HYPO of TMT B and (a) the increase in power of theta band ($|r| > 0.53$, $p < 0.003$ in T6 P4 O2); (b) the increase in power of alpha band ($|r| > 0.58$, $p < 0.001$ in T6 P3 P4 Pz O1 O2); (c) the decrease in power of the beta band ($|r| > 0.54$, $p < 0.003$ in F3 F4 P4 O1 O2) during HYPO in all electrodes.

In particular, we found a significant correlation between the drop in the TMT B performance and:

(a) the increase in the power of theta band in T6-, P4-, O2-A1A2 EEG channels ($|r| > 0.53$, $p < 0.003$);

(b) the increase in power of alpha band in T6-, P3-, P4-, Pz-, O1-, O2-A1A2 ($|r| > 0.58$, $p < 0.001$);

(c) the decrease in power of the beta band in F3-, F4-, P4-, O1-, O2-A1A2 ($|r| > 0.54$, $p < 0.003$).

Fig. 6.6 depicted the results of the magnitude of coefficients $|r|$ (colorbar) between the decrease of Occurrences/s of map D during HYPO:

(a) in theta band and the increase in power of theta band

(b) in beta band and the decrease in power of beta band during HYPO in all electrodes.

Specifically, in (a), we found a significant correlation in the EEG channel Cz-A1A2 ($|r| = 0.59$ ; $p = 0.0007$), while in (b) in Fz-, Cz-A1A2 EEG channels ($|r| > 0.52$ $p < 0.01$).

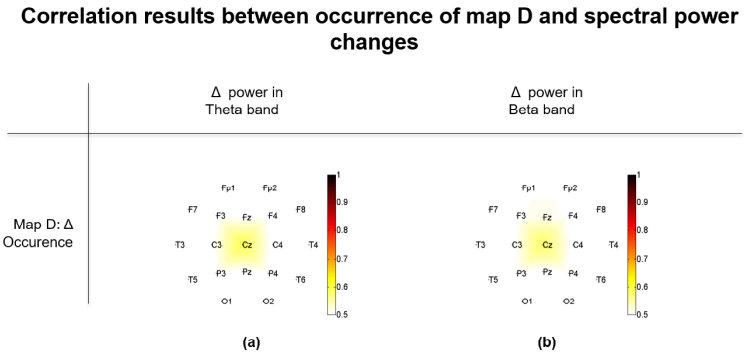


FIGURE 6.6: Results of the magnitude of Pearson's linear correlation coefficients $|r|$ (colorbar) between the decrease of Occurrences/s of map D during HYPO: (a) in theta band and the increase in power of theta band ($|r| = 0.59$ ; $p = 0.0007$ in Cz); (b) in beta band and the decrease in power of beta band ($|r| > 0.52$ $p < 0.01$ in Fz Cz) during HYPO in all electrodes.

## 6.3 Discussion

In this chapter, we checked the interaction of the results presented in the previous Chapters 3 and 5 with the results of the behavioral tests. The generalize slowing proved by the overall

increase in the spectral power of low frequency bands influenced the processing speed and both the visual and selective attention measured by the behavioral tests. Indeed, we found a direct correlation among the changes in the power spectra, the cognitive tests performance and the changes in map D, probably due to the disruption of the cognitive network during HYPO.

# Chapter 7

# Conclusions

## 7.1 Main achievements and discussion

Hypoglycemic events in patients affected by T1D were proved to be associated with measurable EEG changes. In this dissertation, our aim was to have a more complete overview on the effects of hypoglycemia in the brain by broaden the EEG analysis in both the time and frequency domain starting from the literature findings. In particular, we applied our investigation on a database of hospitalized patients who underwent an hyperinsulinemic-hypoglycemic clamp for about 8 h.

As long as modern views of neurology and neuroscience state that the cerebral cortex is based on the dual principle of segregation and integration, i.e., considering functional segregation, the attention is focused on distinct brain areas while taking in account functional integration, the brain does not operate in isolation but by a coordinated activity between different brain areas, we analyzed the EEG changes due to HYPO by different point of views, considering different strategies and methods and considering both all the network and only bipolar EEG channels. In particular, our work was structured with the following goals:

1. Confirming in our data the same effects of HYPO in the

EEG signal demonstrated in the literature, i.e., a generalized slowing of cerebral activity during episodes of HYPO.

2. Proving if this generalize slowing identified by the increase in the spectral power of the low frequency bands was also mirrored in the reduction of EEG complexity, and if it was possible to measure this EEG feature by means of methods with low computational cost.

3. Investigating if these changes in the frequency and complexity domains had in common the same resting EEG electric potential amplitude map.

4. After testing that the state of hypoglycemia influenced the processing speed and both the visual and selective attention, searching a direct correlation among the changes in the power spectra, the cognitive tests performance and the changes in EEG amplitude maps.

It is qualitatively observable by visual inspection that the EEG signal in the hypoglycemic condition originates by a process of higher amplitudes in the low frequency bands and reveals greater regularity (Chapter 2). Indeed (Chapter 3) relative power in both theta and alpha bands statistically increases in HYPO respect to EU. Moreover, the general frequency slowing in HYPO denotes the shifting to lower frequencies of the centroid frequency in alpha band and it is compensated by a significant decrease of power in beta band. In healthy subjects, theta and alpha rhythms usually occur during sleep and/or meditative states while beta waves during alert, problem solving, judgment, decision making, and mental activity. Thus, the increase in low frequency bands parallel to the decrease in fast rhythms most likely is due to the progressive loss of cognitive functions during HYPO.

Actually in our data, this loss of cognitive function during the pathological state of HYPO is proved by the results of TMT B and Stroop tests, where patients in HYPO have a drop in the performance of all the tests. Moreover, how this altered cerebral activity is mainly due to the entering in HYPO and not merely due to tiredness is demonstrated by the equal performance in TMT B and Stroop test in EU before and after the hypoglycemic period (Chapter 6).

After establishing the influence of HYPO in the low EEG rhythms, we investigated how HYPO affects the connectivity between different areas. Our analysis was limited to the temporal, 'central', parietal, and occipital lobes, because we used raw EEG data to avoid to distort the analyses as suggested in the literature. Our results showed that EEG functional connectivity is affected by hypoglycemia in both the theta and alpha bands. In particular, the the value of information Partial Directed Coherence significantly decreased ($p < 0.01$) passing from EU to HYPO from T5-A1A2 to C3-A1A2, from O1-A1A2 to C4-A1A2, and from O2-A1A2 to Cz-A1A2 in the theta band and from O1-A1A2 to T4-A1A2 and from O1-A1A2 to C4-A1A2 in the alpha band. Both T4-A1A2 and O1-A1A2 EEG channels were also involved in the decrease of the value of the centroid frequency in alpha band. Thus, we found a decrease in the connectivity in the path from the occipital lobes to the temporal and central lobes during HYPO (Chapter 3). Probably, the disruption of this piece of brain network during HYPO is the result of the alterations of mental and perceptual functions during the critical state of HYPO. The overall decrease in the value of information Partial Directed Coherence (even if not significant in all combinations of EEG channels) probably confirms the hypothesis that the state of unawareness and unconsciousness due to HYPO disrupts the functional integration of the brain.

To deepen on the analysis on the functional reaction of the brain to HYPO, we also evaluated the degree of complexity taking in account a pair of EEG channels in the posterior area of the brain. In neural signals, complexity is high for systems that contain specialized and organized elements, while it is lower in system uniform or random. Indeed, during HYPO, the EEG signal results more regular, more uniform, less complex respect to EU. This decrease in complexity highlighted by a significant decrease of Higuchi's fractal dimension and an increase of both the new fractal features proposed in our work, confirms the loss in cognitive function during HYPO (Chapter 4).

To complete our insight of the brain state during HYPO, we studied the changes of the brain network dynamics not in the frequency domain, but in the time domain by means of microstates analysis. EEG-resting state can be decomposed into 100-ms time epochs with quasi-stable field topography maps, so called microstates that should correspond to transiently stable distributed neural networks. In our data, map D displayed the more significant differences between the euglycemic and hypoglycemic state. In particular, the total time covered and the occurrences per second of this map during HYPO was lower respect to EU (Chapter 5). Previous studies proved alterations of map D in people with mental disorders compared to healthy controls where map D had a significantly longer mean duration and covered a higher percentage of time [134]. Because of the knowledge of the functional significance of different microstate maps still is very limited, we can only speculate that this evident alteration in map D could be linked with degraded attentional mechanisms caused by HYPO. In a recent study, about the interpretation of the psychological domain described by the microstates maps, they showed that map C becomes more dominant when somatic awareness is reduced [133]. Indeed, comparing the microstates results between

hypo-aware and unaware subjects, we found qualitatively differences in the contribution of map C. Probably due to the limited dataset, we didn't find statistically differences. While in the frequency and cognitive domains, the differences between the two groups were not visible, even qualitatively.

Eventually, evaluating the correlation between the EEG quantitative measures presented in this work, we discovered a similar trend between the results of the spectral power changes in theta, alpha and beta bands and the performance in TMT B and between the theta and beta power changes and the Occurrences/s of map D. For the first relationship, we found a significant correlation between the TMT drop in performance and the power increase of theta and alpha bands and the parallel power decrease of beta band in the posterior area of the brain, probably because this area is responsible for the language and verbal memory that is involved in the cognitive test. While the drop in the Occurrences/s of map D was correlated with the increase in theta power and the decrease of beta power in the central region of the brain, supposed to be the area involved in the cognitive network that seems to be disrupted during HYPO.

## 7.2 Future challenges

In this study, we proved that the well-known low-frequency power increase is specific to a unique large-scale brain network which spatial characteristics still remain to be elucidated by using high-density EEG and electrical source imaging (ESI). ESI is a model-based imaging technique that integrates temporal and spatial components of EEG to identify the generating source of electrical potentials recorded on the scalp [135]. This technique needs an high number of electrodes and possibly, a co-registration of electrode positions on MRI [136]. Identifying the electrical source of

the topographies found during EU and HYPO might help in understanding how the brain is affected by HYPO. Moreover, this technique might validate and deepen the neurological interpretation of the results. Furthermore, the results interpretation could improve by applying the methods presented in this work in extended databases.

Previous studies reported that EEG changes in HYPO suggest a possible use of the brain as a biosensor to detect hypoglycemia in T1D through EEG monitoring by subcutaneous electrodes (with a potential lifetime of several years) and real-time data processing by means of a multi-parameter algorithm [35]. With regard to this aspect, the accuracy achieved in this study may seem far from ideal, but a further investigation of the potential usefulness of EEG in detecting hypoglycemia is still warranted. The benefit of EEG as a biomarker is that the hypoglycemia associated EEG changes are not blunted during hypoglycemia in patients with hypoglycemia unawareness, in contrast to the symptom of hypoglycemia, the counterregulatory hormonal response, and skin temperature changes. By using EEG signals as the measuring principle there is a direct correlation between oncoming hypoglycemia and the signal that is measured. In this way, the measurement principle will be not affected by delays and other unintended transition functions. Furthermore, a frequent calibration as in blood glucose sensors is not required to identify the characteristic hypoglycemia pattern. In particular, authors in [35] focused on the possibility to construct a hypoglycemia alarm system based on continuous EEG monitoring and real-time data processing by means of a multi-parameter algorithm based on four levels, Fig. 7.1. At the first level, the feature extraction based on frequency, amplitude and power of 1-s EEG epoch processes the raw EEG to distinguish EEG altered by hypoglycemia from normal EEG. The second level consists of

three blocks, each of which analyses the features to determine if there is evidence of impending hypoglycemia, deep sleep patterns, or noise contamination, respectively. At the third level, EEG epoch is labeled as consistent or not-consistent with hypoglycemia. Lastly, taking the recent history into account it is determined whether or not a sufficient amount of hypoglycemia evidence is present to constitute an alarm. An EEG-based hypoglycemia detection device, however, still needs to be tested in a clinical setting. Certainly, fundamental issues, such as sensitivity, specificity, reliability, resolution, and influence of activity, must be carefully addressed before demonstrating a real-time usability of such a device. Furthermore, each level of the algorithm presented in Fig. 7.1 should be validated in an extended database and the margins of improvement of each level should be carefully addressed.

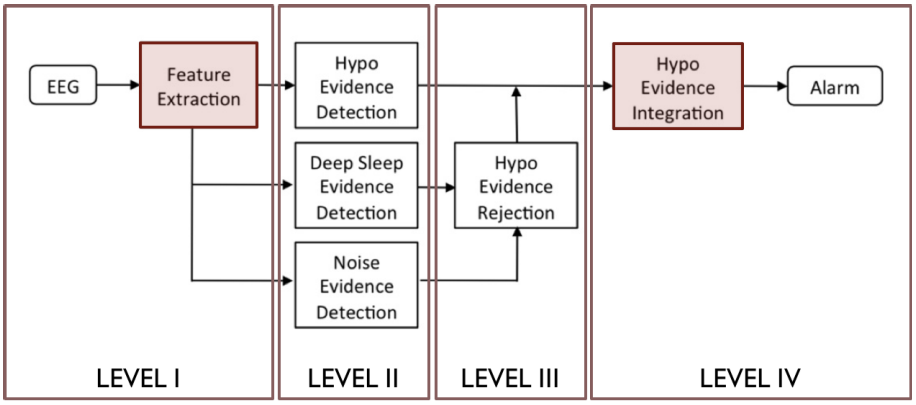


FIGURE 7.1: Structure of the hypoglycemia detection algorithm. Reproduced from [35].

# Bibliography

[1] American Diabetes Association, "Diagnosis and classification of diabetes mellitus", *Diabetes Care*, vol. 33, no. Suppl 1, S62–S69, 2010. DOI: 10.2337/dc10-S062.

[2] J. L. Chiang, M. S. Kirkman, L. M. B. Laffel, and A. L. Peters, "Type 1 diabetes through the life span: A position statement of the american diabetes association", *Diabetes Care*, vol. 37, no. 7, pp. 2034–2054, 2014. DOI: 10.2337/dc14-1140.

[3] J. Tuomilehto, "The emerging global epidemic of type 1 diabetes", *Current Diabetes Reports*, vol. 13, no. 6, pp. 795–804, 2013. DOI: 10.1007/s11892-013-0433-5.

[4] C. C. Patterson, G. G. Dahlquist, E. Gyurus, A. Green, and G. Soltesz, "Incidence trends for childhood type 1 diabetes in europe during 1989-2003 and predicted new cases 2005-20: A multicentre prospective registration study.", *Lancet*, vol. 373, no. 9680, pp. 2027–2033, 2009. DOI: 10.1016/S0140-6736(09)60568-7.

[5] D. Dabelea, "The accelerating epidemic of childhood diabetes", *Lancet*, vol. 373, no. 9680, pp. 1999–2000, 2009. DOI: 10.1016/S0140-6736(09)60874-6.

[6] A. R. Saltiel and C. R. Kahn, "Insulin signaling and the regulation of glucose and lipid metabolism", *Nature*, vol. 414, no. 6865, pp. 799–806, 2001. DOI: 10.1038/414799a.

[7] C. A. J. van Beers and J. H. DeVries, "Analysis: The accuracy and efficacy of the dexcom g4 platinum continuous glucose monitoring system", *Journal of Diabetes Science and Technology*, vol. 9, no. 5, pp. 1027–1029, 2015. DOI: 10.1177/1932296815583508.

[8] R. J. Wright and B. M. Frier, "Vascular disease and diabetes: Is hypoglycaemia an aggravating factor?", *Diabetes/Metabolism Research and Reviews*, vol. 24, no. 5, pp. 353–363, 2008. DOI: 10.1002/dmrr.865.

[9] V. J. Briscoe and S. N. Davis, "Hypoglycemia in type 1 and type 2 diabetes: Physiology pathophysiology and management", *Clinical Diabetes*, vol. 24, no. 3, pp. 115–121, 2006. DOI: 10.2337/diaclin.24.3.115.

[10] B. M. Frier, "Living with hypoglycaemia", in *Hypoglycaemia in Clinical Diabetes*. John Wiley and Sons, Ltd, 2013, pp. 347–368. DOI: 10.1002/9781118695432.ch18.

[11] P. E. Cryer, "Diverse causes of hypoglycemia-associated autonomic failure in diabetes", *N Engl J Med*, vol. 350, no. 22, pp. 2272–2279, 2004. DOI: 10.1056/NEJMra031354.

[12] P. E. Cryer, "The barrier of hypoglycemia in diabetes", *Diabetes*, vol. 57, no. 12, pp. 3169–3176, 2008. DOI: 10.2337/db08-1084.

[13] B. M. Frier, "Hypoglycemia", in *Diabetes and the Brain*, J. G. Biessels and A. J. Luchsinger, Eds. Humana Press, 2010, pp. 131–157. DOI: 10.1007/978-1-60327-850-8_6.

[14] B. M. Frier, "How hypoglycaemia can affect the life of a person with diabetes", *Diabetes/Metabolism Research and Reviews*, vol. 24, no. 2, pp. 87–92, 2008. DOI: 10.1002/dmrr.796.

[15] T. W. Jones, P. Porter, R. S. Sherwin, E. A. Davis, P. O'Leary, F. Frazer, G. Byrne, S. Stick, and W. V. Tamborlane, "Decreased epinephrine responses to hypoglycemia during sleep", *New England Journal of Medicine*, vol. 338, no. 23, pp. 1657–1662, 1998. DOI: 10.1056/NEJM199806043382303.

[16] I. B. Hirsch, S. R. Heller, and P. E. Cryer, "Increased symptoms of hypoglycaemia in the standing position in insulin-dependent diabetes mellitus", *Clinical Science*, vol. 80, no. 6, pp. 583–586, 1991. DOI: 10.1042/cs0800583.

[17] P. McEwan, B. L. Thorsted, M. Wolden, J. Jacobsen, and M. Evans, "Healthcare resource implications of hypoglycemia-related hospital admissions and inpatient hypoglycemia: Retrospective record-linked cohort studies in england", *BMJ Open Diabetes Research and Care*, vol. 3, no. 1, 2015. DOI: 10.1136/bmjdrc-2014-000057.

[18] P. Mergenthaler, U. Lindauer, G. A. Dienel, and A. Meisel, "Sugar for the brain: The role of glucose in physiological and pathological brain function", *Trends in neurosciences*, vol. 36, no. 10, pp. 587–597, 2013. DOI: 10.1016/j.tins.2013.07.001.

[19] F Erbsloh, A Bernsmeier, and H Hillesheim, "[the glucose consumption of the brain & its dependence on the liver].", *Archiv fur Psychiatrie und Nervenkrankheiten, vereinigt mit Zeitschrift fur die gesamte Neurologie und Psychiatrie*, vol. 196, no. 6, pp. 611–626, 1957. DOI: 10.1007/BF00344388.

[20] L. Sokoloff, "Energetics of functional activation in neural tissues", *Neurochemical research*, vol. 24, no. 2, pp. 321–329, 1999. DOI: 10.1023/A:1022534709672.

[21] B. O. Åsvold, T. Sand, K. Hestad, and M. R. Bjørgaas, "Cognitive function in type 1 diabetic adults with early exposure to severe hypoglycemia", *Diabetes Care*, vol. 33, no. 9, pp. 1945–1947, 2010. DOI: 10.2337/dc10-0621.

[22] A.-S. Sejling, T. W. Kjær, U. Pedersen-Bjergaard, S. S. Diemar, C. S. Frandsen, L. Hilsted, J. Faber, J. J. Holst, L. Tarnow, M. N. Nielsen, L. S. Remvig, B. Thorsteinsson, and C. B. Juhl, "Hypoglycemia-associated changes in the electroencephalogram in patients with type 1 diabetes and normal hypoglycemia awareness or unawareness", *Diabetes*, vol. 64, no. 5, pp. 1760–1769, 2015. DOI: 10.2337/db14-1359.

[23] M. Fabrykant and B. L. Pacella, "Association of spontaneous hypoglycemia with hypocalcemia and electrocerebral dysfunction", *Archives of Internal Medicine*, vol. 81, no. 2, pp. 184–202, 1948. DOI: 10.1001/archinte.1948.00220200072008.

[24] I. S. Ross and L. H. Loeser, "Electroencephalographic findings in essential hypoglycemia", in *Electroencephalography and Clinical Neurophysiology*, 2. Elsevier, vol. 3, pp. 141–148. DOI: 10.1016/0013-4694(51)90003-X.

[25] A. Baskaran, R. Milev, and R. S. McIntyre, "A review of electroencephalographic changes in diabetes mellitus in relation to major depressive disorder", *Neuropsychiatric Disease and Treatment*, vol. 9, pp. 143–150, 2013. DOI: 10.2147/NDT.S38720.

[26] O. Eeg-Olofsson and I. Petersen, "Childhood diabetic neuropathy: A clinical and neurophysiological study", *Acta Paediatrica*, vol. 55, no. 2, pp. 163–176, 1966. DOI: 10.1111/j.1651-2227.1966.tb15222.x.

[27] E. Tsalikian, D. J. Becker, P. K. Crumrine, D. Daneman, and A. L. Drash, "Electroencephalographic changes in diabetic ketosis in children with newly and previously diagnosed insulin-dependent diabetes mellitus", *The Journal of Pediatrics*, vol. 99, no. 3, pp. 355–359, 1981. DOI: 10.1016/S0022-3476(81)80317-4.

[28] S Pramming, B Thorsteinsson, B Stigsby, and C Binder, "Glycaemic threshold for changes in electroencephalograms during hypoglycaemia in patients with insulin dependent diabetes.", *British Medical Journal (Clin Res Ed)*, vol. 296, no. 6623, pp. 665–667, 1988.

[29] G Tallroth, M Lindgren, G Stenberg, I Rosen, and C. D. Agardh, "Neurophysiological changes during insulin-induced hypoglycaemia and in the recovery period following glucose infusion in type 1 (insulin-dependent) diabetes mellitus and in normal man", *Diabetologia*, vol. 33, no. 5, pp. 319–323, 1990. DOI: 10.1007/BF00403327.

[30] G Tribl, K Howorka, G Heger, P Anderer, H Thoma, and J Zeitlhofer, "Eeg topography during insulin-induced hypoglycemia in patients with insulin-dependent diabetes mellitus", *European Neurology*, vol. 36, pp. 303–309, 1996. DOI: 10.1159/000117277.

[31] L Hyllienmark, J Maltez, A Dandenell, J Ludvigsson, and T Brismar, "Eeg abnormalities with and without relation to severe hypoglycaemia in adolescents with type 1 diabetes.", *Diabetologia*, vol. 48, no. 3, pp. 412–419, 2005. DOI: 10.1007/s00125-004-1666-2.

[32] C. B. Juhl, K. Hojlund, R. Elsborg, M. K. Poulsen, P. E. Selmar, J. J. Holst, C. Christiansen, and H. Beck-Nielsen, "Automated detection of hypoglycemia-induced eeg changes recorded by subcutaneous electrodes in subjects with type

1 diabetes-the brain as a biosensor.", *Diabetes Research Clinical Practice*, vol. 88, no. 1, pp. 22–28, 2010. DOI: 10.1016/j.diabres.2010.01.007.

[33] [Online]. Available: http://hyposafe.com/.

[34] R. Madsen and H. Beck-Nielsen, *Implantable electronic devices for detecting hypoglycaemia using eeg signals*, US Patent 8,849,368, 2014.

[35] R. Elsborg, L. Remvig, H. Beck-Nielsen, and C. B. Juhl, *Detecting hypoglycemia by using the brain as a biosensor.* InTech, 2011.

[36] L. S. Snogdal, L. Folkestad, R. Elsborg, L. S. Remvig, H. Beck-Nielsen, B. Thorsteinsson, P. Jennum, M. Gjerstad, and C. B. Juhl, "Detection of hypoglycemia associated eeg changes during sleep in type 1 diabetes mellitus", *Diabetes Research and Clinical Practice*, vol. 98, no. 1, pp. 91–97, 2012. DOI: 10.1016/j.diabres.2012.04.014.

[37] U Pedersen-Bjergaard, S Pramming, and B Thorsteinsson, "Recall of severe hypoglycaemia and self-estimated state of awareness in type 1 diabetes", *Diabetes Metabolism Research Reviews*, vol. 19, no. 3, pp. 232–240, 2003. DOI: 10.1002/dmrr.377.

[38] A. E. Gold, K. M. Macleod, and B. M. Frier, "Frequency of severe hypoglycemia in patients with type i diabetes with impaired awareness of hypoglycemia", *Diabetes Care*, vol. 17, no. 7, pp. 697–703, 1994. DOI: 10.2337/diacare.17.7.697.

[39] W. L. Clarke, D. J. Cox, L. A. Gonder-Frederick, D Julian, D Schlundt, and W Polonsky, "Reduced awareness of hypoglycemia in adults with iddm. a prospective study of

hypoglycemic frequency and associated symptoms", *Diabetes Care*, vol. 18, pp. 517–522, 1995. DOI: 10.2337/diacare.18.4.517.

[40] E. A. Gaudino, M. W. Geisler, and N. K. Squires, "Construct validity in the trail making test: What makes part b harder?", *Journal of clinical and experimental neuropsychology*, vol. 17, no. 4, pp. 529–535, 1995. DOI: T10.1080/01688639508405143.

[41] T. N. Tombaugh, "Trail making test a and b: Normative data stratified by age and education", *Archives of clinical neuropsychology*, vol. 19, no. 2, pp. 203–214, 2004. DOI: 10.1016/S0887-6177(03)00039-8.

[42] C. J. Golden, "A group version of the stroop color and word test", *Journal of personality assessment*, vol. 39, no. 4, pp. 386–388, 1975. DOI: 10.1207/s15327752jpa3904_10.

[43] P. L. Kristensen, U. Pedersen-Bjergaard, T. W. Kjær, N. V. Olsen, F. Dela, J. J. Holst, J. Faber, L. Tarnow, and B. Thorsteinsson, "Influence of erythropoietin on cognitive performance during experimental hypoglycemia in patients with type 1 diabetes mellitus: A randomized cross-over trial", *PloS one*, vol. 8, no. 4, e59672, 2013. DOI: 10.1371/journal.pone.0059672.

[44] J. R. Stroop, "Studies of interference in serial verbal reactions.", *Journal of experimental psychology*, vol. 18, no. 6, p. 643, 1935. DOI: 10.1037/h0054651.

[45] L. Blaabjerg and C. B. Juhl, "Hypoglycemia-induced changes in the electroencephalogram: An overview.", *Journal of diabetes science and technology*, pp. 1–9, 2016. DOI: 10.1177/1932296816659744.

[46] G. L. Hansen, P. Foli-Andersen, S. Fredheim, C. Juhl, L. S. Remvig, M. H. Rose, I. Rosenzweig, S. Beniczky, B. Olsen, K. Pilgaard, and J. Johannesen, "Hypoglycemia-associated eeg changes in prepubertal children with type 1 diabetes.", *Journal of diabetes science and technology*, pp. 1–8, 2016. DOI: 10.1177/1932296816634357.

[47] M. Rubega, G. Sparacino, A. S. Sejling, C. B. Juhl, and C. Cobelli, "Hypoglycemia-induced decrease of eeg coherence in patients with type 1 diabetes.", *Diabetes technology & therapeutics*, vol. 18, no. 3, pp. 178–184, 2016. DOI: 10.1089/dia.2015.0347.

[48] C. Fabris, G. Sparacino, A.-S. Sejling, A. Goljahani, J. Duun-Henriksen, L. S. Remvig, C. B. Juhl, and C. Cobelli, "Hypoglycemia-related electroencephalogram changes assessed by multiscale entropy.", *Diabetes technology & therapeutics*, vol. 16, no. 10, pp. 688–694, 2014. DOI: 10.1089/dia.2013.0331.

[49] A. Larsen, K. Hojlund, M. K. Poulsen, R. E. Madsen, and C. B. Juhl, "Hypoglycemia-associated electroencephalogram and electrocardiogram changes appear simultaneously.", *Journal of diabetes science and technology*, vol. 7, no. 1, pp. 93–99, 2013. DOI: 10.1177/193229681300700111.

[50] L. S. Remvig, R. Elsborg, A.-S. Sejling, J. A. Sorensen, L. Sonder Snogdal, L. Folkestad, and C. B. Juhl, "Hypoglycemia-related electroencephalogram changes are independent of gender, age, duration of diabetes, and awareness status in type 1 diabetes.", *Journal of diabetes science and technology*, vol. 6, no. 6, pp. 1337–1344, 2012. DOI: 10.1177/193229681200600612.

[51] K. Howorka, G. Heger, A. Schabmann, P. Anderer, G. Tribl, and J. Zeitlhofer, "Severe hypoglycaemia unawareness is

associated with an early decrease in vigilance during hypoglycaemia", *Psychoneuroendocrinology*, vol. 21, no. 3, pp. 295–312, DOI: 10.1016/0306-4530(95)00034-8.

[52] L. B. Nguyen, A. V. Nguyen, S. H. Ling, and H. T. Nguyen, "Analyzing eeg signals under insulin-induced hypoglycemia in type 1 diabetes patients", in *2013 35th Annual International Conference of the IEEE Engineering in Medicine and Biology Society (EMBC)*, IEEE, 2013, pp. 1980–1983. DOI: 10.1109/EMBC.2013.6609917.

[53] H. T. Nguyen and T. W. Jones, "Detection of nocturnal hypoglycemic episodes using eeg signals", in *2010 Annual International Conference of the IEEE Engineering in Medicine and Biology*, IEEE, 2010, pp. 4930–4933. DOI: 10.1109/IEMBS.2010.5627233.

[54] G. K. Cooray, L. Hyllienmark, and T. Brismar, "Decreased cortical connectivity and information flow in type 1 diabetes", *Clinical Neurophysiology*, vol. 122, no. 10, pp. 1943–1950, 2011. DOI: 10.1016/j.clinph.2011.03.007.

[55] F. Mormann, K. Lehnertz, P. David, and C. E. Elger, "Mean phase coherence as a measure for phase synchronization and its application to the eeg of epilepsy patients", *Physica D: Nonlinear Phenomena*, vol. 144, no. 3, pp. 358–369, 2000. DOI: 10.1016/S0167-2789(00)00087-7.

[56] C. J. Stam, G. Nolte, and A. Daffertshofer, "Phase lag index: Assessment of functional connectivity from multi channel eeg and meg with diminished bias from common sources", *Human brain mapping*, vol. 28, no. 11, pp. 1178–1193, 2007. DOI: 10.1002/hbm.20346.

[57] C. Stam and B. Van Dijk, "Synchronization likelihood: An unbiased measure of generalized synchronization in multivariate data sets", *Physica D: Nonlinear Phenomena*, vol. 163, no. 3, pp. 236–251, 2002. DOI: 10.1016/S0167-2789(01)00386-4.

[58] G. Nolte, A. Ziehe, V. V. Nikulin, A. Schlögl, N. Krämer, T. Brismar, and K.-R. Müller, "Robustly estimating the flow direction of information in complex physical systems", *Physical review letters*, vol. 100, no. 23, p. 234 101, 2008. DOI: 10.1103/PhysRevLett.100.234101.

[59] K. J. Blinowska, "Review of the methods of determination of directed connectivity from multichannel data", *Medical & biological engineering & computing*, vol. 49, no. 5, pp. 521–529, 2011. DOI: 10.1007/s11517-011-0739-x.

[60] D. M. Halliday, "Nonparametric directionality measures for time series and point process data", *Journal of integrative neuroscience*, vol. 14, no. 02, pp. 253–277, 2015. DOI: 10.1142/S0219635215300127.

[61] L. Astolfi, F. Cincotti, D. Mattia, M. G. Marciani, L. A. Baccala, F. D. V. Fallani, S. Salinari, M. Ursino, M. Zavaglia, and F. Babiloni, "Assessing cortical functional connectivity by partial directed coherence: Simulations and application to real data", *IEEE Transactions on Biomedical Engineering*, vol. 53, no. 9, pp. 1802–1812, 2006. DOI: 10.1109/TBME.2006.873692.

[62] M Petti, S Caschera, A Anzolin, J. Toppi, F Pichiorri, F. Babiloni, F. Cincotti, D. Mattia, and L. Astolfi, "Effect of inter-trials variability on the estimation of cortical connectivity by partial directed coherence", in *2015 37th Annual International Conference of the IEEE Engineering in Medicine*

*and Biology Society (EMBC)*, 2015, pp. 3791–3794. DOI: 10.1109/EMBC.2015.7319219.

[63] E. W. Lang, A. M. Tomé, I. R. Keck, J. Górriz-Sáez, and C. G. Puntonet, "Brain connectivity analysis: A short survey", *Computational intelligence and neuroscience*, vol. 2012, p. 8, 2012. DOI: 10.1155/2012/412512.

[64] K. Sameshima and L. A. Baccala, *Methods in brain connectivity inference through multivariate time series analysis*. CRC press, 2014.

[65] [Online]. Available: http://www.scholarpedia.org/article/Brain_connectivity.

[66] M. Reichenbach and P. Morrison, *The direction of time*, 1956.

[67] C. W. Granger, "Investigating causal relations by econometric models and cross-spectral methods", *Econometrica: Journal of the Econometric Society*, pp. 424–438, 1969. DOI: 10.2307/1912791.

[68] L. A. Baccalá and K. Sameshima, "Partial directed coherence: A new concept in neural structure determination", *Biological cybernetics*, vol. 84, no. 6, pp. 463–474, 2001. DOI: 10.1007/PL00007990.

[69] D. Y. Takahashi, L. A. Baccalá, and K. Sameshima, "Information theoretic interpretation of frequency domain connectivity measures", *Biological cybernetics*, vol. 103, no. 6, pp. 463–469, 2010. DOI: 10.1007/s00422-010-0410-x.

[70] L. A. Baccalá, K Sameshima, and D. Takahashi, "Generalized partial directed coherence", in *2007 15th International Conference on Digital Signal Processing*, IEEE, 2007, pp. 163–166. DOI: 10.1109/ICDSP.2007.4288544.

[71] S. M. Kay, *Modern spectral estimation*. NJ: Prentice Hall, 1999.

[72] H. Akaike, *Information theory and an extension of the maximum likelihood principle*. Springer New York, 1998, pp. 199–213. DOI: 10.1007/978-1-4612-1694-0_15.

[73] E. Florin, J. Gross, J. Pfeifer, G. R. Fink, and L. Timmermann, "Reliability of multivariate causality measures for neural data", *Journal of Neuroscience Methods*, vol. 198, no. 2, pp. 344 –358, 2011. DOI: 10.1016/j.jneumeth.2011.04.005.

[74] D. Abásolo, R. Hornero, P. Espino, J. Poza, C. I. Sánchez, and R. de la Rosa, "Analysis of regularity in the eeg background activity of alzheimer's disease patients with approximate entropy", *Clinical Neurophysiology*, vol. 116, no. 8, pp. 1826–1834, 2005. DOI: 10.1016/j.clinph.2005.04.001.

[75] M. Winterhalder, B. Schelter, and J. Timmer, "Detecting coupling directions in multivariate oscillatory systems", *International Journal of Bifurcation and Chaos*, vol. 17, no. 10, pp. 3735–3739, 2007. DOI: 10.1142/S0218127407019664.

[76] L. Faes, G. D. Pinna, A. Porta, R. Maestri, and G. Nollo, "Surrogate data analysis for assessing the significance of the coherence function", *IEEE transactions on biomedical engineering*, vol. 51, no. 7, pp. 1156–1166, 2004. DOI: 10.1109/TBME.2004.827271.

[77] C. S. N. de Brito, L. A. Baccalá, D. Y. Takahashi, and K. Sameshima, "Asymptotic behavior of generalized partial directed coherence", in *2010 Annual International Conference of the IEEE Engineering in Medicine and Biology*, IEEE, 2010, pp. 1718–1721. DOI: 10.1109/IEMBS.2010.5626856.

[78] L. B. Nguyen, A. V. Nguyen, S. H. Ling, and H. T. Nguyen, "Combining genetic algorithm and levenberg-marquardt algorithm in training neural network for hypoglycemia detection using eeg signals.", *Conference proceedings : Annual International Conference of the IEEE Engineering in Medicine and Biology Society. IEEE Engineering in Medicine and Biology Society*, vol. 2013, pp. 5386–5389, 2013. DOI: 10.1109/EMBC.2013.6610766.

[79] F Laione and J. Marques, "Methodology for hypoglycaemia detection based on the processing, analysis and classification of the electroencephalogram", *Medical and Biological Engineering and Computing*, vol. 43, no. 4, pp. 501–507, 2005. DOI: 10.1007/BF02344732.

[80] A. Goljahani, C. D'Avanzo, S Schiff, P. Amodio, P Bisiacchi, and G. Sparacino, "A novel method for the determination of the eeg individual alpha frequency", *NeuroImage*, vol. 60, no. 1, pp. 774–786, 2012. DOI: 10.1016/j.neuroimage.2011.12.001.

[81] U. R. Acharya, K. P. Joseph, N. Kannathal, C. M. Lim, and J. S. Suri, "Heart rate variability: A review", *Medical and biological engineering and computing*, vol. 44, no. 12, pp. 1031–1051, 2006. DOI: 10.1007/s11517-006-0119-0.

[82] J Escudero, D Abásolo, R Hornero, P Espino, and M López, "Analysis of electroencephalograms in alzheimer's disease patients with multiscale entropy", *Physiological measurement*, vol. 27, no. 11, p. 1091, 2006. DOI: 10.1088/0967-3334/27/11/004.

[83] M., A. L. Goldberger, and C.-K. Peng, "Multiscale entropy analysis of complex physiologic time series", *Physical review letters*, vol. 89, no. 6, p. 068 102, 2002. DOI: 10.1103/PhysRevLett.89.068102.

[84] J. S. Richman and J. R. Moorman, "Physiological time-series analysis using approximate entropy and sample entropy.", *American journal of physiology. Heart and circulatory physiology*, vol. 278, no. 6, H2039–49, 2000.

[85] L. Ji, P. Li, C. Liu, X. Wang, J. Yang, and C. Liu, "Measuring electromechanical coupling in patients with coronary artery disease and healthy subjects", *Entropy*, vol. 18, no. 4, p. 153, 2016. DOI: 10.3390/e18040153.

[86] O. Faust, U. R. Acharya, F. Molinari, S. Chattopadhyay, and T. Tamura, "Linear and non-linear analysis of cardiac health in diabetic subjects", *Biomedical Signal Processing and Control*, vol. 7, no. 3, pp. 295–302, 2012. DOI: 10.1016/j.bspc.2011.06.002.

[87] S. Farashi, "A multiresolution time-dependent entropy method for qrs complex detection", *Biomedical Signal Processing and Control*, vol. 24, pp. 63–71, 2016. DOI: 10.1016/j.bspc.2015.09.008.

[88] H. Azami and J. Escudero, "Improved multiscale permutation entropy for biomedical signal analysis: Interpretation and application to electroencephalogram recordings", *Biomedical Signal Processing and Control*, vol. 23, pp. 28–41, 2016. DOI: 10.1016/j.bspc.2015.08.004.

[89] C. Fabris, W. De Colle, and G. Sparacino, "Voice disorders assessed by (cross-) sample entropy of electroglottogram and microphone signals", *Biomedical Signal Processing and Control*, vol. 8, no. 6, pp. 920–926, 2013. DOI: 10.1016/j.bspc.2013.08.010.

[90] U. R. Acharya, F. Molinari, S. V. Sree, S. Chattopadhyay, K.-H. Ng, and J. S. Suri, "Automated diagnosis of epileptic eeg using entropies", *Biomedical Signal Processing and*

*Control*, vol. 7, no. 4, pp. 401–408, 2012. DOI: 10.1016/j.bspc.2011.07.007.

[91] S. Simons, D. Abasolo, and J. Escudero, "Classification of alzheimer's disease from quadratic sample entropy of electroencephalogram", *Healthcare technology letters*, vol. 2, no. 3, p. 70, 2015. DOI: 10.1049/htl.2014.0106.

[92] L. Faes, G. Nollo, and A. Porta, "Compensated transfer entropy as a tool for reliably estimating information transfer in physiological time series", *Entropy*, vol. 15, no. 1, pp. 198–219, 2013. DOI: 10.3390/e15010198.

[93] M. Ronzhina, O. Janoušek, J. Kolářová, M. Nováková, P. Honzík, and I. Provazník, "Sleep scoring using artificial neural networks", *Sleep medicine reviews*, vol. 16, no. 3, pp. 251–263, 2012. DOI: 10.1016/j.smrv.2011.06.003.

[94] A. Accardo, M Affinito, M Carrozzi, and F Bouquet, "Use of the fractal dimension for the analysis of electroencephalographic time series", *Biological cybernetics*, vol. 77, no. 5, pp. 339–350, 1997. DOI: 10.1007/s004220050394.

[95] G. Polychronaki, P. Ktonas, S Gatzonis, A Siatouni, P. Asvestas, H Tsekou, D Sakas, and K. Nikita, "Comparison of fractal dimension estimation algorithms for epileptic seizure onset detection", *Journal of neural engineering*, vol. 7, no. 4, p. 046 007, 2010. DOI: 10.1088/1741-2560/7/4/046007.

[96] F. Finotello, F. Scarpa, and M. Zanon, "Eeg signal features extraction based on fractal dimension", in *2015 37th Annual International Conference of the IEEE Engineering in Medicine and Biology Society (EMBC)*, IEEE, 2015, pp. 4154–4157. DOI: 10.1109/EMBC.2015.7319309.

[97] T. Higuchi, "Approach to an irregular time series on the basis of the fractal theory", *Physica D: Nonlinear Phenomena*, vol. 31, no. 2, pp. 277–283, 1988. DOI: 10.1016/0167-2789(88)90081-4.

[98] R. Ferenets, T. Lipping, A. Anier, V Jantti, S. Melto, and S. Hovilehto, "Comparison of entropy and complexity measures for the assessment of depth of sedation", *IEEE Transactions on Biomedical Engineering*, vol. 53, no. 6, pp. 1067–1077, 2006. DOI: 10.1109/TBME.2006.873543.

[99] T. Takahashi, R. Y. Cho, T. Murata, T. Mizuno, M. Kikuchi, K. Mizukami, H. Kosaka, K. Takahashi, and Y. Wada, "Age-related variation in eeg complexity to photic stimulation: A multiscale entropy analysis", *Clinical Neurophysiology*, vol. 120, no. 3, pp. 476–483, 2009. DOI: 10.1016/j.clinph.2008.12.043.

[100] T. Mizuno, T. Takahashi, R. Y. Cho, M. Kikuchi, T. Murata, K. Takahashi, and Y. Wada, "Assessment of eeg dynamical complexity in alzheimer's disease using multiscale entropy", *Clinical Neurophysiology*, vol. 121, no. 9, pp. 1438–1446, 2010. DOI: 10.1016/j.clinph.2010.03.025.

[101] T. Takahashi, R. Y. Cho, T. Mizuno, M. Kikuchi, T. Murata, K. Takahashi, and Y. Wada, "Antipsychotics reverse abnormal eeg complexity in drug-naive schizophrenia: A multiscale entropy analysis", *Neuroimage*, vol. 51, no. 1, pp. 173–182, 2010. DOI: 10.1016/j.neuroimage.2010.02.009.

[102] A. Catarino, O. Churches, S. Baron-Cohen, A. Andrade, and H. Ring, "Atypical eeg complexity in autism spectrum conditions: A multiscale entropy analysis", *Clinical neurophysiology*, vol. 122, no. 12, pp. 2375–2383, 2011. DOI: 10.1016/j.clinph.2011.05.004.

[103] R. A. Thuraisingham and G. A. Gottwald, "On multiscale entropy analysis for physiological data", *Physica A: Statistical Mechanics and its Applications*, vol. 366, pp. 323–332, 2006. DOI: 10.1016/j.physa.2005.10.008.

[104] B. Klinkenberg, "A review of methods used to determine the fractal dimension of linear features", *Mathematical Geology*, vol. 26, no. 1, pp. 23–46, 1994. DOI: 10.1007/BF02065874.

[105] M. Bachmann, J. Lass, A. Suhhova, and H. Hinrikus, "Spectral asymmetry and higuchi's fractal dimension measures of depression electroencephalogram", *Computational and mathematical methods in medicine*, vol. 2013, 2013. DOI: 10.1155/2013/251638.

[106] F. Scarpa, X. Zheng, Y. Ohashi, and A. Ruggeri, "Automatic evaluation of corneal nerve tortuosity in images from in vivo confocal microscopy", *Investigative ophthalmology & visual science*, vol. 52, no. 9, pp. 6404–6408, 2011. DOI: 10.1167/iovs.11-7529.

[107] S.-D. Wu, C.-W. Wu, S.-G. Lin, K.-Y. Lee, and C.-K. Peng, "Analysis of complex time series using refined composite multiscale entropy", *Physics Letters A*, vol. 378, no. 20, pp. 1369–1374, 2014. DOI: 10.1016/j.physleta.2014.03.034.

[108] D Lehmann, H Ozaki, and I Pal, "Eeg alpha map series: Brain micro-states by space-oriented adaptive segmentation", *Electroencephalography and clinical neurophysiology*, vol. 67, no. 3, pp. 271–288, 1987. DOI: 10.1016/0013-4694(87)90025-3.

[109] A. Khanna, A. Pascual-Leone, C. M. Michel, and F. Farzan, "Microstates in resting-state eeg: Current status and future directions", *Neuroscience & Biobehavioral Reviews*, vol.

49, pp. 105–113, 2015. DOI: 10.1016/j.neubiorev.2014.12.010.

[110] R. D. Pascual-Marqui, C. M. Michel, and D. Lehmann, "Segmentation of brain electrical activity into microstates: Model estimation and validation", *IEEE Transactions on Biomedical Engineering*, vol. 42, no. 7, pp. 658–665, 1995. DOI: 10.1109/10.391164.

[111] M. M. Murray, D. Brunet, and C. M. Michel, "Topographic erp analyses: A step-by-step tutorial review", *Brain topography*, vol. 20, no. 4, pp. 249–264, 2008. DOI: 10.1007/s10548-008-0054-5.

[112] C. M. Michel, *Electrical neuroimaging*. Cambridge University Press, 2009.

[113] T. Koenig, L. Prichep, D. Lehmann, P. V. Sosa, E. Braeker, H. Kleinlogel, R. Isenhart, and E. R. John, "Millisecond by millisecond, year by year: Normative eeg microstates and developmental stages", *Neuroimage*, vol. 16, no. 1, pp. 41–48, 2002. DOI: 10.1006/nimg.2002.1070.

[114] M. E. Raichle, A. M. MacLeod, A. Z. Snyder, W. J. Powers, D. A. Gusnard, and G. L. Shulman, "A default mode of brain function", *Proceedings of the National Academy of Sciences*, vol. 98, no. 2, pp. 676–682, 2001. DOI: 10.1073/pnas.98.2.676.

[115] T Dierks, V Jelic, P Julin, K Maurer, L. Wahlund, O Almkvist, W. Strik, and B Winblad, "Eeg-microstates in mild memory impairment and alzheimer's disease: Possible association with disturbed information processing", *Journal of neural transmission*, vol. 104, no. 4-5, pp. 483–495, 1997. DOI: 10.1007/BF01277666.

[116] D. Lehmann, P. L. Faber, S. Galderisi, W. M. Herrmann, T. Kinoshita, M. Koukkou, A. Mucci, R. D. Pascual-Marqui, N. Saito, J. Wackermann, *et al.*, "Eeg microstate duration and syntax in acute, medication-naive, first-episode schizophrenia: A multi-center study", *Psychiatry Research: Neuroimaging*, vol. 138, no. 2, pp. 141–156, 2005. DOI: 10.1016/j.pscychresns.2004.05.007.

[117] M. Kikuchi, T. Koenig, T. Munesue, A. Hanaoka, W. Strik, T. Dierks, Y. Koshino, and Y. Minabe, "Eeg microstate analysis in drug-naive patients with panic disorder", *PLoS One*, vol. 6, no. 7, e22912, 2011. DOI: 10.1371/journal.pone.0022912.

[118] A. Stevens and T. Kircher, "Cognitive decline unlike normal aging is associated with alterations of eeg temporo-spatial characteristics", *European archives of psychiatry and clinical neuroscience*, vol. 248, no. 5, pp. 259–266, 1998. DOI: 10.1007/s004060050047.

[119] D. Lehmann, R. D. Pascual-Marqui, W. K. Strik, and T. Koenig, "Core networks for visual-concrete and abstract thought content: A brain electric microstate analysis", *Neuroimage*, vol. 49, no. 1, pp. 1073–1079, 2010. DOI: 10.1016/j.neuroimage.2009.07.054.

[120] W. J. Krzanowski and Y. Lai, "A criterion for determining the number of groups in a data set using sum-of-squares clustering", *Biometrics*, pp. 23–34, 1988. DOI: 10.2307/2531893.

[121] M. Charrad, N. Ghazzali, V. Boiteau, A. Niknafs, and M. M. Charrad, "Package 'nbclust'", *Journal of Statistical Software*, vol. 61, pp. 1–36, 2014.

[122] G. W. Milligan and M. C. Cooper, "An examination of procedures for determining the number of clusters in a data set", *Psychometrika*, vol. 50, no. 2, pp. 159–179, 1985. DOI: 10.1007/BF02294245.

[123] J. C. Bezdek and N. R. Pal, "Some new indexes of cluster validity", *IEEE Transactions on Systems, Man, and Cybernetics, Part B (Cybernetics)*, vol. 28, no. 3, pp. 301–315, 1998. DOI: 10.1109/3477.678624.

[124] M. Charrad, Y. Lechevallier, M. B. Ahmed, and G. Saporta, "On the number of clusters in block clustering algorithms.", in *FLAIRS Conference*, 2010.

[125] W. Sarle, "Sas technical report a-108", *The Cubic Clustering Criterion. Cary, NC: SAS Institute*, 1983.

[126] D. Brunet, M. M. Murray, and C. M. Michel, "Spatiotemporal analysis of multichannel eeg: Cartool", *Computational intelligence and neuroscience*, vol. 2011, p. 2, 2011. DOI: 10.1155/2011/813870.

[127] Y. Benjamini and D. Yekutieli, "The control of the false discovery rate in multiple testing under dependency", *The Annals of Statistics*, vol. 29, no. 4, pp. 1165–1188, 2001. DOI: 10.1214/aos/1013699998.

[128] E. L. Vlahou, F. Thurm, I.-T. Kolassa, and W. Schlee, "Resting-state slow wave power, healthy aging and cognitive performance", *Scientific Reports*, vol. 4, 5101 EP –, 2014. DOI: 10.1038/srep05101.

[129] L. M. Ward, "Synchronous neural oscillations and cognitive processes", *Trends in cognitive sciences*, vol. 7, no. 12, pp. 553–559, 2003. DOI: 10.1016/j.tics.2003.10.012.

[130] A. K. Engel and P. Fries, "Beta-band oscillations—signalling the status quo?", *Current opinion in neurobiology*, vol. 20, no. 2, pp. 156–165, 2010. DOI: 10.1016/j.conb.2010.02.015.

[131] M. J. Kahana, D. Seelig, and J. R. Madsen, "Theta returns", *Current opinion in neurobiology*, vol. 11, no. 6, pp. 739–744, 2001. DOI: 10.1016/S0959-4388(01)00278-1.

[132] A.-L. Giraud and D. Poeppel, "Cortical oscillations and speech processing: Emerging computational principles and operations", *Nature neuroscience*, vol. 15, no. 4, pp. 511–517, 2012. DOI: 10.1038/nn.3063.

[133] E. Pipinis, S. Melynyte, T. Koenig, L. Jarutyte, K. Linkenkaer-Hansen, O. Ruksenas, and I. Griskova-Bulanova, "Association between resting-state microstates and ratings on the amsterdam resting-state questionnaire", *Brain Topography*, pp. 1–4, 2016. DOI: 10.1007/s10548-016-0522-2.

[134] T. Koenig, D. Lehmann, M. C. Merlo, K. Kochi, D. Hell, and M. Koukkou, "A deviant eeg brain microstate in acute, neuroleptic-naive schizophrenics at rest", *European archives of psychiatry and clinical neuroscience*, vol. 249, no. 4, pp. 205–211, 1999. DOI: 10.1007/s004060050088.

[135] R. D. Pascual-Marqui, C. M. Michel, and D. Lehmann, "Low resolution electromagnetic tomography: A new method for localizing electrical activity in the brain", *International Journal of psychophysiology*, vol. 18, no. 1, pp. 49–65, 1994. DOI: 10.1016/0167-8760(84)90014-X.

[136] C. M. Michel, M. M. Murray, G. Lantz, S. Gonzalez, L. Spinelli, and R. G. de Peralta, "Eeg source imaging", *Clinical neurophysiology*, vol. 115, no. 10, pp. 2195–2222, 2004. DOI: 10.1016/j.clinph.2004.06.001.